

---


Electronic Theses and Dissertations, 2004-2019

---

2006

## Lattice Vibration Study Of Silica Nanoparticle In Suspension

Parveen Sachdeva  
*University of Central Florida*

 Part of the [Mechanical Engineering Commons](#)  
Find similar works at: <https://stars.library.ucf.edu/etd>  
University of Central Florida Libraries <http://library.ucf.edu>

This Masters Thesis (Open Access) is brought to you for free and open access by STARS. It has been accepted for inclusion in Electronic Theses and Dissertations, 2004-2019 by an authorized administrator of STARS. For more information, please contact [STARS@ucf.edu](mailto:STARS@ucf.edu).

---

### STARS Citation

Sachdeva, Parveen, "Lattice Vibration Study Of Silica Nanoparticle In Suspension" (2006). *Electronic Theses and Dissertations, 2004-2019*. 838.  
<https://stars.library.ucf.edu/etd/838>

LATTICE VIBRATION STUDY OF SILICA NANOPARTICLE IN SUSPENSION

by

PARVEEN SACHDEVA  
B.Tech. Indian Institute of Technology Kanpur, 2003

A thesis submitted in partial fulfillment of the requirements  
for the degree of Master of Science  
in the Department of Mechanical, Materials and Aerospace Engineering  
in the College of Engineering and Computer Science  
at the University of Central Florida  
Orlando, Florida

Summer Term  
2006

© 2006 Parveen Sachdeva

## **ABSTRACT**

In recent years considerable research has been done in the area of “nanofluids”. Nanofluids are colloidal suspensions of nanometer size metallic or oxide particles in a base fluid such as water, ethylene glycol. Nanofluids show enhanced heat transfer characteristics compared to the base fluid. The thermal transport properties of nanofluids depend on various parameters e.g. interfacial resistance, Brownian motion of particles, liquid layering at the solid-liquid interface and clustering of nanoparticles. In this work atomic scale simulation has been used to study possible mechanisms affecting the heat transfer characteristics of nanofluids. Molecular dynamics simulation for a single silica nanoparticle surrounded by water molecules has been performed. Periodic boundary condition has been used in all three directions. The effect of nanoparticle size and temperature of system on the thermal conductivity of nanofluids has been studied. It was found that as the size of nanoparticle decreases thermal conductivity of nanofluid increases. This is partially due to the fact that as the diameter of nanoparticle decreases from micrometer to nanometer its surface area to volume ratio increases by a factor of  $10^3$ . Since heat transfer between the fluid and the nanoparticle takes place at the surface this enhanced surface area gives higher thermal conductivity for smaller particles. Thermal conductivity enhancement is also due to the accumulation of water molecules near the particle surface and the lattice vibration of the nanoparticle. The phonon transfer through the second layer allows the nanofluid thermal conductivity to increase by 23%-27% compared to the base fluid water for 2% concentration of nanosilica.

Dedicated to my sisters Ritu, Poonam and my parents Asha and Jagdish

## ACKNOWLEDGMENTS

This work and my stay at UCF has been a great learning experience for me. I would like to take this opportunity to express gratitude to my advisor Dr. R. Kumar for his constant support, advice and guidance throughout my stay at UCF. It was a rewarding experience working with him. I am thankful to Dr. X. Wu for his endless help, which came at a time when it was badly needed. I also acknowledge and offer thanks to my committee members Dr. J. Kapat and Dr. R. Guha for their valuable comments and guidance. I also acknowledge the support of the College of Engineering & Computer Science and the I<sup>2</sup>Lab at the University of Central Florida for the research presented here.

I would also like to thank my friends at UCF for making my stay memorable. I thank the UCF Indian student association, *Sangam* for their help when I first came to USA.

None of this would have been possible without the blessings of Nirankari Baba Hardev Singh Ji and the constant support and encouragement of my family members and my best friend Vasud.

## TABLE OF CONTENTS

LIST OF FIGURES .....	viii
LIST OF TABLES .....	ix
LIST OF ABBREVIATIONS.....	x
CHAPTER 1: INTRODUCTION .....	1
1.1 Potential Applications.....	3
1.2 Problem Description .....	4
CHAPTER 2: LITERATURE REVIEW .....	7
2.1 Experimental Results for Nanofluids.....	7
2.2 Modeling of Nanofluids.....	10
2.3 Literature Review on Molecular Dynamics Simulation .....	16
CHAPTER 3: METHODOLOGY .....	40
3.1 Molecular Dynamics Simulation .....	42
3.2 Potential Functions used in Simulation.....	50
3.2.1 Interactions in Silica Nanoparticle.....	50
3.2.2 Liquid-Liquid Interaction.....	51
3.2.3 Solid-Liquid Interaction.....	53
3.2.4 Coulombic Interaction .....	54
3.3 Generation of Nanoparticle.....	57
3.4 Molecular Dynamics Simulation of Thermal Conductivity.....	59
CHAPTER 4: PARALLEL MOLECULAR DYNAMICS.....	60
4.1 Atom decomposition algorithm .....	64

4.2 Spatial decomposition method.....	66
4.3 Simulation Procedure.....	70
CHAPTER 5: RESULTS AND DISCUSSION.....	72
5.1 Lattice Vibration of the Nanoparticle.....	72
5.2 Density Profile near the Interface.....	73
5.3 Heat Current Autocorrelation Function.....	77
5.4 Thermal Conductivity Enhancement.....	78
CHAPTER 6: CONCLUSION.....	83
CHAPTER 7: FUTURE WORK.....	85
LIST OF REFERENCES.....	87



## LIST OF FIGURES

Figure 1: Silica nanoparticle surrounded by water molecules .....	5
Figure 2: Silica nanoparticle surrounded by water molecules .....	6
Figure 3: Schematic of the simulation domain used in NEMD simulation by Wu & Kumar .....	19
Figure 4: Simulation techniques for various length and time scales .....	40
Figure 5: General flowchart of MD algorithm.....	43
Figure 6: Potential energy of a particle in LJ model.....	45
Figure 7: Neighbor-list construction with radius $r_{list}$ .....	49
Figure 8: Structure of water molecule in SPC/E model.....	52
Figure 9: Generating the nanoparticles from Silica unit-cell.....	58
Figure 10: 1nm and 2nm diameter silica nanoparticles .....	58
Figure 11: Flowchart of parallel molecular dynamics code.....	65
Figure 12: Smoothed density profiles of water for 1nm and 2nm nanoparticle at T=300K.....	74
Figure 13: Density of water molecules higher close to the surface compared to far away .....	75
Figure 14: Schematic nanoparticle surrounded by liquid layer [Yu and Choi, 2003] .....	76
Figure 15: Heat current autocorrelation function.....	78
Figure 16: Thermal conductivity of water, nanoparticle and nanofluid at 300K.....	80
Figure 17: Thermal conductivity of 1nm and 2nm nanofluid and pure water at T=300K.....	81

## LIST OF TABLES

Table 1: Thermal conductivities of various materials at 300K.....	2
Table 2: MD work related to thermal conductivity calculation.....	23
Table 3: MD work related to modeling of water molecule.....	27
Table 4: Force field parameters for silica nanoparticle .....	51
Table 5: Calculated thermal conductivity of 3 nanofluids at various temperatures .....	81

## LIST OF ABBREVIATIONS

$k_e$	Effective thermal conductivity
$k_f$	Thermal conductivity of fluid
$k_p$	Thermal conductivity of particle
$\alpha$	$k_f/k_p$
$\phi$	Volume fraction of particles
$\phi$	Volume fraction of particles
$n$	non-spherical shape factor
$\psi$	Sphericity
$J_\mu$	Thermal current
$T$	Temperature
$\partial T / \partial x$	Temperature gradient
$\nabla$	Gradient
$f_i$	Force on atom $i$
$\phi$	Interatomic potential
$q_i$	Charge on atom $i$
$E_k$	Electric field at site $k$
$\mu$	Dipole moment
$erf$	error function
$q(t)$	Heat current
$\lambda$	Thermal conductivity

## CHAPTER 1: INTRODUCTION

Heating and cooling fluids are of major importance in many industries including transportation, micro-electronics, manufacturing, production, energy supply and metrology. Other important uses of heat transfer fluids include vehicular and avionics cooling systems, hydraulic heating and cooling systems in buildings, and industrial process heating and cooling systems in petrochemical, textile, food and other processing plants. Heat transport characteristics of these fluids are vital in designing and developing high efficiency heat transfer equipments. Thermal conductivity of these fluids plays an important role in the development of these devices. Low thermal conductivity of these fluids hinders high effectiveness and compactness of heat exchangers and other devices. High heat flux is produced in smaller (<100 nm) microelectronic devices, in high speed devices (in GHz range), in brighter optical devices and in high power output engines. Conventional heat transfer methods use extended surfaces such as fins to increase heat transfer rates, but contemporary designs are already stretched to their limits and no improvements have been made in this area for the last few years using conventional methods. With the advent of nanotechnology, size of many devices is decreasing while the heat flux produced by these devices is increasing. Researchers around the world are looking for efficient ways to remove high heat fluxes out of the miniature devices. Therefore, there is an urgent need to develop advanced heat transfer fluids with higher thermal conductivity and enhanced heat transport characteristics.

Researchers have been working for decades to develop more efficient heat transfer fluids but their efforts are constrained because of low thermal conductivity of conventional fluids. It is well

known that crystalline solids e.g. metals and oxides at room temperature have several orders-of-magnitude high thermal conductivity compared to conventional heat transfer fluids also thermal conductivity of metallic liquids is higher compared to non-metallic liquids. For example, thermal conductivity of copper is 650 times and that of silicon is 240 times higher than that of water as shown in Table 1. Therefore, it is expected that thermal conductivity of liquids suspended with metallic or oxide particles should be significantly higher compared to the base fluid.

Table 1: Thermal conductivities of various materials at 300K

<b>Material</b>	<b>Thermal Conductivity (W/mK)</b>	<b>Specific Thermal Conductivity</b>
Silver	429	700
Copper	401	654
Aluminum	237	387
Silicon	148	241
Liquid Sodium at 644K	72.3	118
Silica ( $\alpha$ quartz)	8.2	13.37
Water	0.613	1
Ethylene glycol	0.253	0.41
Engine Oil	0.145	0.24

Numerous theoretical and numerical studies have been done to calculate the effective thermal conductivity of suspensions consisting of solid particles in base liquid. However earlier studies on thermal conductivity calculation of dispersions of solid particles in liquid were confined to

millimeter and micrometer size particles. Ahuja [1975] studied suspension of sub-micron size polystyrene particles in ethylene glycol and showed that the heat transfer was increased by a factor of 2 under laminar flow conditions and negligible difference in pressure drop was observed even for particle volume fraction of 9%. [Liu et al., 1988] also found enhanced heat transfer in particulate slurries. These studies used were micron-sized particles. A major drawback of micron-sized particles is that they settle down quickly and pose significant corrosion and abrasion hazards in engineering fluid systems. The settling of these micron-sized particles can also cause clogging and result in higher pressure drop for the flow. Even though the suspensions of these particles have higher thermal conductivity compared to their base fluids, they have little application in engineering systems due to the problems associated with them. With the advent of nanotechnology, researchers have been able to manufacture nano-sized particles. Application of nanoparticles provides an effective way of increasing thermal conductivity of fluids. These nanoparticles due to their small size are highly stable in suspensions and do not settle down quickly. So these nanoparticles overcome the shortcoming posed by micron-sized particles and show exciting possibility of enhancing heat transport properties of conventional heat transfer fluids.

### **1.1 Potential Applications**

The potential application of this research work in many industries makes it a compelling study. Even at low loading levels, nanofluids dramatically increase the thermal conductivity and critical heat flux and therefore can be used in many practical applications. These nanofluids can be used in transportation industry as coolants and heat removing lubricants in the automobiles. They can

be used in chip cooling industry and electronic packaging industry where high heat flux emanates from the devices. These could be used to design highly efficient portable cooling systems, and portable power generation systems. Nanofluids can help design thermal systems with precise temperature control. The nanofluids can be used in space applications also, they will reduce the quantity of required cooling fluid onboard, and resulting in a weight reduction of both ground and space based instruments. The nanofluids will also help improve the thermal performance of miniaturized heat transport devices that are designed for applications such as cooling small sensors and MEMS devices. They can also be used as liquid cooling systems for super computers and server systems. The use of nanofluids is currently evaluated in industries that deal with very high heat fluxes, e.g. nuclear reactors and laser systems.

## **1.2 Problem Description**

From the numerous experimental and computational studies we understand that nanofluids show promise in enhancing heat transfer characteristics of conventional fluids. Many theories and mechanism at the molecular level have been proposed which explains the heat transfer characteristics of nanofluids. Where such studies are available, results have not been encouraging, the thermal conductivity enhancement by using nanofluids is still not predicted with a great deal of accuracy. To use it in industry or engineering systems we should have some theory or correlations to predict their performance or efficiency. The experiments are not always reproducible and there is no validation of experimental results conducted by various researchers around the world. These thermal characteristics of nanofluids depend on many parameters i.e. volume concentration, size, shape and material of nanoparticle, No systematic study has been

done till now to find the effects of various parameters. In this work, a systematic study of nanoparticle size and temperature is performed using the molecular dynamics simulation. The results calculated from this simulation will be shown to be consistent with experimental results. To study the effect of nanoparticle size and system temperature silica nanoparticle surrounded by water molecules is simulated using atomic scale simulation.

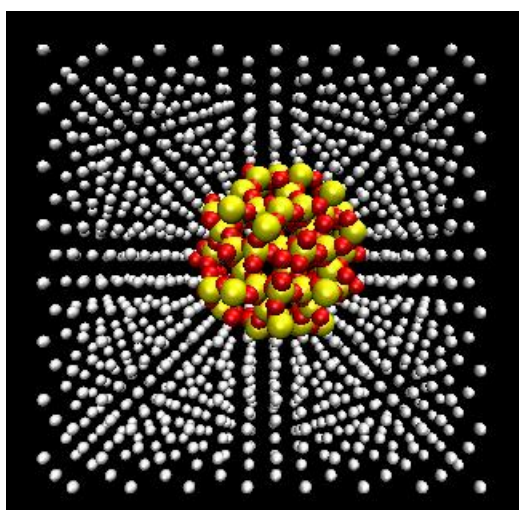


Figure 1: Silica nanoparticle surrounded by water molecules

Figure 1 shows the simulation domain which consists of a silica nanoparticle of 1.5 nm diameter surrounded by water molecules in a cube of length 4.02 nm. Water molecules in the simulation assumes tetrahedral structure with  $r_{O-H}=0.1\text{nm}$  and  $\angle HOH = 109.47^\circ$ . For clarity the water molecules is shown as a monatomic particle in Figure 1. Figure 2 shows the tetrahedral water molecules near the surface of nanoparticle. Hydrogen, oxygen and silicon atoms are represented by white, red and yellow colors respectively.



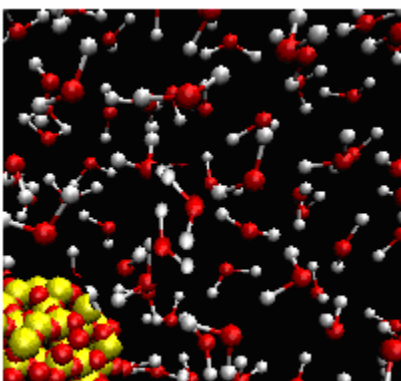


Figure 2: Silica nanoparticle surrounded by water molecules

The objective of this work is to study the transport mechanisms occurring in nanofluids using atomic scale simulation. Molecular dynamics (MD) simulation will be used to study the phenomenon occurring at the atomic scale. The proposed tasks for this work are:

**Task 1:** Develop MD code to study the interaction between nanoparticles surrounded by water molecules.

**Task 2:** Parallelize the code using the atom decomposition method.

**Task 3:** Study the effect of nanoparticle size and system temperature on thermal conductivity of nanofluid.

## **CHAPTER 2: LITERATURE REVIEW**

### **2.1 Experimental Results for Nanofluids**

Masuda et al [1993] were the first ones to do experiments with suspension of nanoparticles and report enhanced heat transfer. They reported 30% increase in thermal conductivity of water suspended with alumina nanoparticles at a volume fraction of 4.3%. Choi at Argonne national lab engineered a new class of fluids with enhanced heat transfer characteristics and was the first one to call these colloidal suspensions nanofluids [Choi, 1995] which is now commonly accepted. Lee et al [1999] did experimental study of alumina and cupric oxide nanoparticles suspended in water and ethylene glycol and found 15% enhancement in the thermal conductivity of alumina-water nanofluid at the same volume fraction as Masuda et al. The difference in the results was attributed to the size of nanoparticles, Masuda et al used 13nm alumina nanoparticles while Lee et al used 33nm nanoparticles. Wang et al [1999] studied the effect of particle size and volume fraction on the thermal conductivity of nanofluids. They showed that thermal conductivity of nanofluids increases with decreasing particle size for nanofluids consisting of alumina and cupric oxide nanoparticles suspended in water and ethylene glycol. Thermal conductivity increases with increasing particle volume fraction. They observed a maximum of 12% thermal conductivity rise for alumina nanoparticles with a volume fraction of 3%. Eastman et al [2001] reported anomalously increased thermal conductivity for ethylene glycol suspended with copper nanoparticles. They reported 40% enhancement in the thermal conductivity of ethylene glycol suspended with only 10nm copper nanoparticles at 0.3% volume fraction. Earlier, they observed 20% increase in thermal conductivity with 4% volume fraction of 35nm

cupric oxide nanoparticles. This clearly shows the effect of the size of particle and also shows that metallic particles give enhanced thermal conductivity compared to oxide particles. Das et al [2003] used temperature oscillation technique to study the effect of temperature on the thermal conductivity of alumina and cupric oxide nanoparticles in water. They measured thermal conductivity at temperatures ranging from 20°C to 50°C for different volume fraction and reported a linear increase in thermal conductivity with increased temperature. Patel et al [2003] reported similar trends for 4nm gold nanoparticles suspended in toluene. They even showed that for the same surface area to volume fraction ratio, we can get different conductivities when the materials are different. Several researchers [Jang and Choi, 2004, Vassallo et al., 2004, Milanova and Kumar, 2005] have reported significant increase in critical heat flux in pool boiling heat transfer experiments consisting of nanofluids. All these exciting properties make nanofluids promising for next generation thermal-management systems. Milanova et al, [2006] experimentally studied the heat transfer characteristics of silica ( $\text{SiO}_2$ ), ceria ( $\text{CeO}_2$ ) and alumina ( $\text{Al}_2\text{O}_3$ ) nanofluids at 0.5% concentration. They studied the effect of surface chemistry of nanoparticles, pH of the nanofluid solution, agglomeration of nanoparticles and effect of particle size by using 10nm and 20nm nanoparticles in pool boiling experiment. They found that the critical heat flux (CHF) increased by about 50% regardless of particle size and type when no particles were deposited on the heating wire. The boiling regime is further extended to higher heat flux when there is nanoparticle agglomeration on the heating wire. The nanoparticle agglomeration on the wire causes high heat transfer from the inter-agglomerate pores, resulting in nearly 150% increase in CHF. The deposition of nanoparticles was seen for charged 10nm silica nanoparticles, while ceria and alumina nanoparticles did not show any deposition on the wire. The oxygen vacancies present in nano-ceria cause the natural convection regime to depart

faster to the nucleate boiling regime, compared to silica and alumina. Ceria nanofluid shows lower CHF compared to alumina and silica nanofluids. The smallest silica particles (10nm diameter) showed highest deposition on the wire and highest CHF enhancement, which suggests that the porosity due to silica deposition and oxidation of the Nichrome heating wire are responsible for the greatest increase in CHF. Milanova and Kumar [2006] also studied the effect of surface charge of silica nanoparticles using the zeta-potential technique on the heat transfer enhancement of the silica-water nanofluid. Unlike the previously postulated theory that the CHF monotonically increases with increasing particle concentration they found that the CHF can increase or decrease with increasing particle concentration depending on the particle shape and the hydroxylated surface of the nanoparticle. By using the particle sizing they showed the formation of an ordered second fixed layer (hydration layer) on the surface of nanoparticle. This ordered layer is formed by the hydrogen bonds between the silanol group ( $\text{Si}_{\text{surface}}\text{OH}:\text{OH}_2$ ) with water molecules. The size and the curvature of the particles determine the extent of hydration layer. Bigger particles possess more silanol groups, which provide higher repulsive force between nanoparticles and hence less agglomeration. The zeta potential measurement for 20nm and 10nm silica nanoparticle shows that the bigger particle has higher negative potential ( $\xi_{20\text{nm}} = -27\text{mV}$ ,  $\xi_{10\text{nm}} = -23.5\text{mV}$ ). It was observed that the size of 10nm particle increased to 18nm and 20nm for 1% and 2% volume concentration respectively. Four regions based on nanoparticle concentration were observed. In region 1 (0.1-0.2% conc.), the particle size remains constant because no agglomeration occurs and the CHF slightly increases. In region 2 (0.2-0.5% conc.), the particle size increases from to almost twice in diameter due to agglomeration and the surface density decreases. But the rate of increase of surface area is higher than rate of decrease of number density and so CHF increases. In region 3 (0.5-1.0% conc.), the size of nanoparticle

increases to double the diameter and then remains constant and the number density decreases. In this region the rate of decrease in number density is higher than the rate of increase of surface area and so the CHF decreases in this region. In region 4 (1.0-2.0% conc.) the particle size after agglomeration remains constant and CHF increases because the particle concentration is increasing. So it was shown that the CHF of nanofluid depends not only on the particle concentration and size but also on particle shape, agglomeration characteristics and the hydroxylated surface of the nanoparticle.

It is well known that carbon nanotubes (CNT) exhibit unusually high thermal conductivities [Berber et al., 2000]. Choi et al extended the idea of nanoparticle suspension to suspension of CNT's in oil [Choi et al., 2001]. Since carbon is hydrophobic so it can not be dispersed in water without additional surfactants. They reported 250% increase in thermal conductivity at 1% volume fraction of multiwall carbon nanotubes (MWNT) having 25nm mean diameter and 50 $\mu$ m length. Xie et al reported only 20% increase in thermal conductivity with MWNT suspension in poly oil [Xie et al., 2003]. It was shown that unlike nanoparticles, suspension of nanotubes show quadratic variation with volume fraction.

## **2.2 Modeling of Nanofluids**

It is evident that a lot of research has been conducted in determining the heat transport characteristics of the nanofluids in last decade. But still many questions remain unanswered. The data produced by one group is not reproducible by another and no concrete theory has been established to calculate the thermal conductivity of nanofluids and explain this phenomenon.

Researchers have proposed many theories to explain the anomalous behavior observed in nanofluids. The early attempts to explain the enhanced transport characteristics of nanofluids were made with the classical theory of Maxwell [1881] for composite materials. This theory is applicable for dilute suspension of spherical particles in homogeneous isotropic composite material.

$$\frac{k_e}{k_f} = 1 + \frac{3\phi(\alpha - 1)}{(\alpha + 2) - \phi(\alpha - 1)} \quad (2.1)$$

Here  $k_e$  is the effective thermal conductivity of the suspension,  $k_f$  is the thermal conductivity of the base fluid,  $\alpha$  is the ratio of thermal conductivity of the particle to that of the fluid,  $\phi$  is the volume fraction. It is appropriate for predicting properties such as thermal conductivity, electrical conductivity, dielectric constant and magnetic permeability of composite materials. When compared with experimental data Maxwell's theory matched well for low particle concentrations with particles of millimeter or micrometer size. But it did not conform well to particles of smaller size and non-spherical shapes.

Hamilton and Crosser [1962] (H-C) extended Maxwell's theory and generalized it for non-spherical particles. They came up with an expression for effective thermal conductivity of a colloidal suspension as:

$$\frac{k_e}{k_f} = \frac{\alpha + (n - 1)[1 + \phi(\alpha - 1)]}{\alpha + (n - 1) - \phi(\alpha - 1)} \quad (2.2)$$

Here,  $n$  is the non-spherical shape factor given as:

$$n = 3/\psi \quad (2.3)$$

Here  $\psi$  is the sphericity, defined as the ratio of the surface area of a sphere with volume equal to that of the particle to the surface area of the particle. For  $n=3$  this equation becomes the Maxwell equation for spherical particles. The HC theory was used by Xuan and Li [2000] to obtain rough estimation of thermal conductivity of nanofluids for different volume fraction and shape factor. They showed that for  $\psi=0.7$  the model predicts results close to the experimental results. Lee *et al* [1999] showed that H-C theory predicted the right trend for oxide particles, but when used for very fine metallic particles [Eastman et al, 2001] it under-predicted the effective thermal conductivity by over an order of magnitude. H-C theory takes into account the increase in surface area of the particles by taking the shape factor into account, but it does not consider the size of the particles. This is an obvious shortcoming of this theory. H-C takes into account only the volume fraction of particles and shape but it does not include the effect of size and material of particle used and the temperature of nanofluid. It was not surprising that both Maxwell's theory and HC theory were not able to predict the enhancement in thermal conductivity of nanofluids because it did not take into account the various important parameters affecting the heat transport in nanofluids like the effect of size of nanoparticle and modes of thermal transport in nanostructures.

Kablinski et al [2002] attribute the enhancement in thermal conductivity to four possible mechanisms, Brownian motion of particles, layering of liquid molecules around the particles, ballistic nature of heat transport in nano-structures and nanoparticle clustering. Particles move through liquid by Brownian motion and collide with each other, hence enabling direct solid-solid transport of heat from one to another. Bhattacharya *et al* [2004] carried out Brownian dynamics

simulation with equilibrium Green-Kubo method to calculate effective thermal conductivity of nanofluid and found good agreement with experimental results. But their results depend on the correlated parameters which were used to match with experimental data and are difficult to apply in other nanofluid simulations as there is no systematic way to find these parameters. Although initial calculations [Bhattacharya et al, 2004] showed significant increases in thermal conductivity from Brownian motion of particles, interaction parameters based on appropriate Debye length increased the conductivity by less than 2% [Gupta et al, 2006]. Koblinski et al did an order of magnitude analysis between thermal diffusion and Brownian diffusion and showed that even for extremely small particles thermal diffusion is much faster than Brownian diffusion, so they concluded that Brownian effects are small in heat transport in nanofluids. It was also observed that liquid molecules near the surface of solid particle form an ordered layer around it, thereby enhancing the local ordering. Since phonon transfer in solids is very effective, this local ordering enhances the heat transport from solid to liquid. These results have been confirmed by Sachdeva *et al* [2005]. Liquid layering around the particle is an important phenomenon affecting the thermal conductivity but it is not the sole reason for the thermal conductivity enhancement in the nanofluids. Another mechanism proposed by Koblinski et al was that nature of heat transport in nano-structure is not diffusive but ballistic in nature. If the ballistic phonons initiated in one particle can persist in liquid and be transmitted to another particle, this can significantly improve the heat transfer. The phononic nature of heat transport originating from lattice vibrations in solid particle was also reported by Wu *et al* [2006]. Lattice vibrations in solid particles combined with liquid layering around the particle and Brownian motion of the particles can be termed as significant mechanisms for the heat transfer enhancement in nanofluids. Lastly it was suggested that if nanoparticles form clusters, thereby increase the overall diameter of the cluster and



decrease the thermal conductivity. Local clustering of particles has been observed experimentally also by Eastman and co-workers [Eastman et al, 2001, Eastman et al, 1999]. Keblinski *et al* [2002] used a single particle surrounded by fluid molecules to carry out equilibrium molecular dynamics (MD) simulation. Lennard-Jones potential was used to simulate the interactions between all atoms, and the interactions inside the nanoparticle were ten times higher than those between fluid atoms. Their simulation revealed the basic phenomena, no quantitative information on the extent of heat transfer enhancement was provided, however this could be due to the fact that appropriate potential were not used to induce lattice vibration. Therefore, they never realized thermal conductivity enhancement of more than 2%. Wu and Kumar [2004] used non-equilibrium molecular dynamics (NEMD) method to calculate the thermal conductivity of nanofluid. They considered all the possible interactions, fluid-fluid, particle-particle and fluid-particle possible in a nanofluid suspension. They used L-J like potential to simulate the fluid-fluid and fluid-particle interactions and another inter-atomic potential is used for particle-particle interactions. The particle-particle potential takes into account the diameter of the particles also. They used perfectly elastic collisions between particles to simulate the non-agglomerated case and perfectly inelastic collision method to simulate to agglomeration between nanoparticles. The results for non-agglomerated system match fairly well with the experimental results for nanofluid consisting of 10nm copper nanoparticles with water. The random Brownian motion of particles show a strong dependence on temperature and the frequency of collision between fluid molecules and nanoparticle increases with temperature, therefore the effective thermal conductivity of the suspension also increases. It was also observed that the agglomeration between nanoparticles decreases the heat transfer enhancement, particularly at low concentration, since the agglomerated particles tend to settle down in liquid and also reduce the number density

of particles, which creates large regions of particle-free liquid. It was also shown that the effective thermal conductivity of nanofluid decreases as the number of agglomerated nanoparticles increases. Although this work used simple potential functions to simulate the interactions and the whole nanoparticle was also considered as single atom/particle, but this work gives good insight into the difference between agglomerated and non-agglomerated system and the results also match with experiments. In another work Wu and Kumar [2005] used a mesoscopic thermal lattice Boltzmann model to study the fluid flow and heat transfer process of nanofluids in a microchannel. Effect of various internal and external forces, such as buoyancy, gravity, drag and Brownian force was also taken into account. The double-distribution-function (DDF) was used to simulate flow process and temperature distribution of nanofluids in a channel. It was observed that the suspended nanoparticles are in random motion along with the streamwise flow due to the various internal and external forces. The distribution morphology of nanoparticles plays an important role in convective heat transfer enhancement of nanofluid. Due to the random motion of the nanoparticles the temperature distribution in case of nanofluid is quite different from that of pure fluid flowing through a channel. The temperature distribution for nanofluid is irregular and it becomes flatter in the vertical direction compared to the pure fluid case. This flattened temperature distribution results in a more effective heat transfer efficiency of the nanofluid. Distribution of the suspended nanoparticles leads to a fluctuation of the Nusselt number of the nanofluids in the direction of the main flow, but the average value of Nusselt number for the laminar flow of nanofluid in a channel shows an increase compared to that for pure fluid under the same condition.

Other attempts have also been made to model heat transport in nanofluids. Yu and Choi [2003] modified Maxwell's equation to include the effect of liquid layering around the particle and found good match with experimental data. They came up with an expression for  $K_e$ :

$$k_e = \frac{k_{pe} + 2k_1 + 2(k_{pe} - k_1)(1 + \beta)^3\phi}{k_{pe} + 2k_1 - (k_{pe} - k_1)(1 + \beta)^3\phi} k_1 \quad (2.4)$$

Here,  $K_e$  is the effective thermal conductivity of nanofluid,  $K_{pe}$  is the equivalent thermal conductivity of equivalent nanoparticles and  $\beta$  is the ratio of the nano-layer thickness to the original particle radius. To simplify their analysis they assumed that thermal conductivity of nano-layer is same as that of the particle. They concluded that the ordered liquid layer around the nanoparticles effectively increases the particle volume fraction and hence the effective thermal conductivity of the nanofluids.

Although lot of work has gone in studying the mechanisms of heat transport in nanofluids there is no set theory for the same. There is a need to systematically study the various mechanisms postulated by researchers to understand the phenomenon occurring at nanoscale heat transfer.

### **2.3 Literature Review on Molecular Dynamics Simulation**

Molecular dynamics (MD) is a very powerful computer simulation technique where the time evolution of a set of interacting atoms is studied by integrating their equations of motion. MD essentially involves solving a classical many-body problem in the context of the study of matter at the atomic scale. It allows predicting the static and dynamic properties of the system under consideration. For complex systems which are modeled poorly by continuum or analytical

methods, Molecular Dynamics (MD) simulation lends itself as a very good computational tool. MD has been used to support research in the areas of physics, chemistry, biology and material science. Alder and Wainwright [1959] were amongst the first ones to do MD simulation in 1959 at the Lawrence Livermore National Laboratory. They used a “hard sphere” model to study the molecules in liquid which interact as “billiard balls”. They were able to simulate 32 and 108 molecules in computations requiring 10 to 30 hours with the fastest computers at that time, an IBM 704. Rahman [1964] studied many properties of liquid argon using Lennard-Jones potential on a system containing 864 atoms. Verlet [1967] calculated the phase diagram of argon using L-J potential and computed correlation functions to test theories of liquid state. Most of systems studied at that time contained very small number of atoms but now with improvements in computer architecture it is possible to simulate million of particles but the computations are very demanding.

Table 2 shows the work done in the area of thermal conductivity calculation using computer experiments. Table 3 gives a list of publications showing various models to simulation water molecule in a MD simulation. These tables discuss equilibrium molecular dynamics (EMD), non-equilibrium molecular dynamics (NEMD) and various models for the simulation of water molecules at the atomic scale. Experimentally, thermal conductivity ( $\lambda$ ) is typically calculated by measuring the temperature gradient that results from the application of a heat current. The thermal conductivity relates the heat current to the temperature gradient via Fourier’s law as:

$$J_{\mu} = -\sum_{\nu} \lambda_{\mu\nu} \frac{\partial T}{\partial x_{\nu}} \quad (2.5)$$

Where  $J_\mu$  is a component of the thermal current,  $\lambda_{\mu\nu}$  is an element of the thermal conductivity tensor, and  $\partial T/\partial x_\nu$  is the gradient of the temperature. In MD simulations the thermal conductivity can be computed either using the non-equilibrium MD (NEMD) or equilibrium MD (EMD) methods. The two most commonly applied methods in MD are the ‘direct method’ and the Green-Kubo method. The direct method is an NEMD method in which a temperature gradient across the simulation cell, essentially mimicking the experimental situation. On the other hand, in the EMD method we use the Green-Kubo correlations which use the heat current fluctuations to compute the thermal conductivity via the fluctuation-dissipation theorem.

The NEMD or direct method of computing the thermal conductivity is analogous to the experimental measurement. Wu and Kumar [2004] used NEMD method to calculate the thermal conductivity of suspension of copper nanoparticles in water. Figure 3 shows a schematic representation of the simulation domain used to compute  $\lambda$  by Wu and Kumar [2004]. The simulation domain is divided into 10 layers with each layer having identical thickness and volume. Layer 0 was divided into 2 equidistant parts to be consistent with the periodic boundary condition. Layer 0 is defined as the “cold” layer and layer 5 as the “hot” layer (Figure 3). The initial temperature of whole system is maintained somewhere in between  $T_H$  and  $T_L$ .

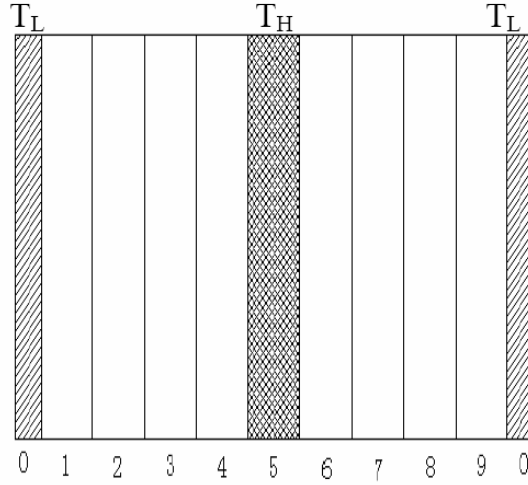


Figure 3: Schematic of the simulation domain used in NEMD simulation by Wu & Kumar

By exchanging the particles (fluid molecules and nanoparticles) with highest velocity in cold layer with the ones having lowest velocity in hot layer, the heat flux is generated in the system. By exchanging the velocities in this way the temperature in the hot layer increases and in the cold layer decreases, setting an temperature gradient in the system. This temperature gradient leads to an energy transfer from the hot layer to the cold layer by heat conduction. Total momentum, kinetic energy and total energy are maintained constant in this exchange process.

When the system reaches steady state, the heat flow due to velocity exchange of particles must equal the heat conduction from the hot layer to the cold layer in both directions. The energy balance can be written as:

$$\sum_{i=0,1} \sum_{transfer} \frac{m_i}{2} (v_{i,h}^2 - v_{i,c}^2) = -2\lambda t A_{yz} \frac{\partial T}{\partial x} \quad (2.6)$$

Where,  $m_i$  is the mass of the particle ( $i=0, 1$  refer to the fluid molecule and nanoparticle respectively),  $v_h$  and  $v_c$  are the velocity of particles in hot and cold layers respectively,  $A_x$  is the cross section area of calculated domain and  $t$  is the thickness of the layer. All the quantities in equation (2.4) are exactly known, except the temperature gradient. The temperature gradient has to be calculated using the kinetic theory of gases, which relates temperature with velocity of particles as follows:

$$T_k = \frac{1}{3n_i k_B} \sum_i \sum_{j=1}^{n_i} m_i v_{j,i}^2 \quad (2.7)$$

Where  $T_k$  is the instantaneous local temperature of layer  $k$ ,  $n_i$  is the number of  $i^{\text{th}}$  particle in layer  $k$ ,  $v_{j,i}$  is the velocity of  $i^{\text{th}}$  particle in layer  $k$ , and  $k_B$  is the Boltzmann's constant. Using the velocities calculated at each MD time step we can calculate the temperature of hot and cold layer and then calculate the temperature gradient. The left hand side of equation (2.6) is known and by plugging in the temperature gradient we can calculate the thermal conductivity of the simulation domain.

As we observe in Figure 3, the application of hot and cold layer (source and sink) and application of periodic boundary condition only generates a heat current in the x-direction and with a single simulation thermal conductivity only along one particular direction can be calculated. To obtain  $\lambda$  along a different crystal lattice direction, an entirely new simulation domain with layers along the required lattice direction must be created and new simulation must be carried out. This limitation does not exist for the Green-Kubo method, where the entire thermal conductivity tensor is computed in just one simulation. For the direct method, it is important that a steady-state heat current flow has been achieved. This can be achieved by plotting a stationary

temperature profile as a function of time, thus insuring that only steady-state currents are flowing and, hence thermal conductivity can be computed using equation (2.6).

In EMD simulation, Green-Kubo correlations are used to compute the thermal conductivity. In EMD simulation there is no imposed driving force on the system, and hence the system is always in the linear-response regime. Since the simulation is done in equilibrium and the system response in the linear regime, according to the fluctuation-dissipation theorem, the transport coefficients can be calculated using the Green-Kubo correlations. In this method the heat current autocorrelation function is calculated and is correlated to the thermal conductivity via the Green-Kubo expression:

$$\lambda = \frac{1}{3K_BVT^2} \int_0^{\infty} \langle q(0).q(t) \rangle dt \quad (2.8)$$

Where  $V$  is the system volume,  $t$  is time and  $q$  is the heat current, and the angular brackets denote an ensemble average, or, in the case of MD simulation it denotes an average over time. The heat current  $q$  is defines as:

$$q = \frac{d}{dt} \sum_i r_i(t) E_i(t) \quad (2.9)$$

Where  $r_i(t)$  is the time-dependent coordinate of atom  $i$  and  $E_i(t)$  is the total energy of atom  $i$ .

Total energy for each atom  $i$  is defined as:

$$E_i(t) = \frac{1}{2} m_i v_i^2 + \frac{1}{2} \sum_j u_2(r_{ij}) \quad (2.10)$$

Here the first term is the kinetic energy and second term is the potential energy of atom  $i$ , and  $u_2(r_{ij})$  is the pairwise interaction. Plugging equation (2.10) in (2.9) the expression for heat current becomes:



$$q(t) = \sum_i v_j E_i + \frac{1}{2} \sum_{ij, i \neq j} r_{ij} (F_{ij} \cdot v_i) \quad (2.11)$$

Where  $F_{ij}$  is the force on atom  $i$  due to its neighboring atoms  $j$  calculated using the pair potentials.

As mentioned earlier one advantage of Green-Kubo method over the NEMD method is that we can calculate complete conductivity tensor in one simulation and it is useful to study the anisotropic effects in the thermal conductivity. In case of direct method or NEMD we will have to run 3 separate simulations to calculate conductivity in 3 directions. Table 2 shows the work done in the area of thermal conductivity calculation using computer experiments.

Table 2: MD work related to thermal conductivity calculation

No.	Author / Journal / Year	Title	Simulation Details	Comments
1	Vagelsang, Hoheisel, Ciccotti. J. Chem. Phy. 1987	Thermal conductivity of LJ liquid by MD calculation	EMD used. Effect of number of particles and truncation of potential considered.	EMD results compared well with previous NEMD results. $k$ independent of MD conditions, reason arises from short ranged time decay of correlation function. For states take, the pair correlation function involving the ‘potential- potential’ term governs the transport coefficient. Large number of particles in simulation gives better results.
2	Lee et. al. Phy. Rev. B 1991	MD simulation of thermal conduction in amorphous Si	EMD relating $k$ to time correlation of heat flux operator. WWW model and SW potential used.	$K(T)$ increases at low temperatures (below 400 K). For $T > 400$ K, $k(T)$ is affected by the thermally generated coordination defects. For $50 < T < 800$ K, $k(\text{of } a\text{-Si})$ increases, consistent with experiments. Difference in calculated and experimental data values because of absence of long-wavelength propagating phonon modes in calculation with mfp larger than cell size.
3	Tsuji et. al.	Movement of	Morse	Virtual electron do not interact with

		free electron in order to simulate thermodynamics by electron current	potential for Cu. Virtual electrons used. Introduce electrons as virtual particles in simulation domain.	each other and have perfectly elastic collision with other atoms. $r_{\text{virtual}}$ and $m_{\text{electron}}$ can be changed to fix other parameters. Heat transfer in metal and electric current can be effectively simulated with this method.
4	Schelling et. al. Phy. Rev. B 2002	Comparison of atomic level simulation for computing thermal conductivity	EMD & NEMD compared. SW Si used. Both methods show finite size effects.	G-K EMD results are insensitive to definition of local energy from many body part of potential. EMD/NEMD results consistent with experiments. EMD gives linear response even for high T gradient, NEMD gives non-linear response. Large simulation time is an issue for EMD. GK desirable for systems with larger mfp e.g. Si. For system with grain boundary direct method preferred.
5	McGaughey, Kaviany. J. Heat Mass Tr. 2004	Thermal conductivity decomposition and analysis using MD I: LJ	EMD with Green-Kubo. LJ Ar (fcc)	1 <sup>st</sup> t scale: phonons with mfp < $0.5*\lambda$ . $k \sim 0.09$ W/mK, independent of T. 2 <sup>nd</sup> t scale: phonons with mfp > $0.5*\lambda$ . $k \sim 3.92$ W/mK for T ~ 10 K and 0.08 W/mK for T ~ 100 K.

				<p>1<sup>st</sup> mode decay time ~ time required for energy transfer from one atom to other.</p> <p>2<sup>nd</sup> mode decay time ~ average decay of phonons with mfp &gt; 0.5*λ.</p>
6	McGaughey, Kaviany. J. Heat Mass Tr 2004	Thermal conductivity decomposition and analysis using MD II: Complex Silica Structure	BKS potential with LJ used for Silica	<p>1<sup>st</sup> mechanism of thermal transport, short range, mfp &gt; 0.5*λ. T independent, <math>k \sim 1</math> W/mK. Governed by Si coordination number.</p> <p>2<sup>nd</sup> mechanism, long range, T dependent, mfp &gt; 0.5*λ.</p> <p>At 300 K, c-direction of quartz: <math>k \sim 9</math> W/mK, zeolite-A: <math>k \sim 0.4</math> W/mK. Controlled by atomic bond length and angles.</p>
7	Tokumasu, Kamijo. Superlattices and microstructures 2004	MD study of thermal conductivity of diatomic liquid	<p>NEMD</p> <p>O<sub>2</sub>, CO, CS<sub>2</sub>, Cl<sub>2</sub>, Br<sub>2</sub></p> <p>2CLJ</p> <p><math>T_{cr}</math>, <math>P_{cr}</math>, <math>\rho_{cr}</math> determined.</p>	<p>Equation of state of each liquid determined using MD.</p> <p>Simulation results in 10% of experimental.</p> <p><math>k_{reduced} = f(k, T_{cr}, \rho_{cr}, m)</math>. <math>k_{red}</math> increases as molecular elongation increases.</p> <p>Contribution of <math>q</math> caused by energy transport and by translational energy transfer to <math>k</math> is independent of molecular elongation.</p> <p>Contribution of <math>q</math> by rotational energy to <math>k</math> increases with increasing molecular elongation.</p>

				$k$ increases as $\rho$ increases or $P$ increases.
8	Eastman et. al. Annu. Rev. Mat. Research 2004	Thermal transport in nanofluids	As size decreases $A_s/V$ inc. Surfactants improve $k$ .	Size of nanoparticle important for heat transfer at $s-f$ interface. Particle agglomeration undesirable. Dispersion improves with non-agglomeration. Particle surface treatment is important. Temperature effects need to be determined.
9	Mensah et. al. Physica E 2004	High electron thermal conductivity of chiral CNT	BKE, TB, CCNT	At $T=104$ K, Overlap integrals $\Delta_Z = 0.02$ eV, $\Delta_S = 0.015$ eV. $K_c = 41,000$ W/mK for 99.97% pure $^{12}\text{C}$ .
10	Tretiakov, Scandolo. J. Chem. Phy 2004	Thermal conductivity of solid Ar from MD	EMD, GK, LJ	Results in agreement with experiment, contrary to previous work. Simplified models for the thermal conductivity based on high T limit of 3-phonon scattering rate reproduce author's data well. Size effects negligible in GK approach for $k$ .

Table 3 gives a list of publications showing various models to simulation water molecule in a MD simulation.

Table 3: MD work related to modeling of water molecule

No	Author / Journal / Year	Title	Simulation Details	Comments
1	Stillinger, Rahman J. Chem. Phy. 1974	Improved simulation of water by MD	5-site, 4-charge ST-2 model used.	ST-2 is comparatively improved to BNS. Modification improves the fidelity of MD. Results for molecular structure and thermodynamic properties show improved quality compared to previous potentials used for water.
2	Matsuoka, Clemeti, yoshimine. J. Chem. Phy. 1976	CI study of the water dimer potential surface	Potential energies for water dimer in various configurations examined.	Ab initio method is used. Ground state wave-function is written.
3	Jorgensen, Chandrashekhar , Madura. J. Chem. Phy. 1983	Comparison of simple potential for simulating water	BF, SPC, ST2, TIPS2, TIP3P, TIP4P. H <sub>2</sub> O at 25 °C and 1 atm.	Results compare well except for BF model. TIPS2 and TIP4P give good results for O-O partial structure functions, H-H and O-H results are poorer.

			NPT ensemble.	SPC, ST2, TIPS2 and TIP4P give good results for thermodynamic and structural properties.
4	Jorgensen. J. Chem. Phy. 1986	Optimized intermolecular Potential function for liquid Alcohols	Thermodynamic and structural results reported. Potential functions have been developed for Alcohols and other molecules with hydroxyl groups.	Optimization done with the study of five alcohols. The five alcohols show winding hydrogen-bonded chains. Hydrogen bonding also shows effects on torsional energy surfaces for molecules in the liquids. Narrowing of conformational energy wells for rotation about C-O bond is also reported. Excellent accord of computation results and experimental results is found.
5	Berendsen, Grigera and Straatsma J. Chem. Phy. 1987	The missing terms in effective pair potentials (SPC/E)	Density, RDF and diffusion constant have been computed and show improvement	The missing self energy term has been included in the effective pair potential of polarizable liquid. The inclusion of this term in the SPC method gives improved results for simulation of liquid water.

			over previous results.	
6	Dang and Pettitt. J. Chem. Phy. 1987	Simple intermolecular model potential for water	3-Site model. 216 water molecules. Cube of 18.6 Å side. Density 1 g/cm <sup>3</sup> . Transition frequency and spectral shifts reported.	Agreement with ground vibrational state frequency. A full quasi-harmonic-mode analysis on the dynamic liquid state trajectories can be performed with this model. Model useful in large solute aqueous simulation.
7	Anderson, Ullo, Yip. J. Chem. Phy. 1987	MD simulation of dielectric properties of water	Time correlation function of dipole moment and single molecular orientation evaluated. Other structural	Water monomer as flexible molecule with short range interaction between O-H. SPC and ST2 better than MCY and TIP4P. Good agreement for self diffusion and satisfactory agreement for static dielectric constant found.



			properties examined.	
8	Zhenqin, Scheraga. J. Chem. Phy – 1989	Monte Carlo recursion study of cluster formation from vapor	NPT ensemble used. Gibbs free energy of cluster formation observed.	Cluster formation from monoatomic vapor observed. Gibbs free energy of a cluster in a constrained equilibrium with vapor is calculated.
9	Koplik, Banavar, Willemsen. Phy. of Fluids A 1989	MD of fluid flow at solid surface.	Fluid-wall interaction examined.	At normal density in couette and poiseuille flow no-slip boundary condition observed. Slip appears at lower densities. This can be incorporated into a flow- independent slip length boundary condition. Trajectories of independent molecules are examined and their average behavior can be given with Taylor-axis hydrodynamics dispersion.

10	Matsumoto, Maruyama. JSME-KSME 1992	Far infrared spectrum of water by MD simulation.	ST2 potential is used. Pure rotational spectra of water observed.	Molecular motion under 3 states liquid, vapor and cluster is observed. Shape of rotational spectrum is simply the reflection of angular velocity for gas case. Effect of free rotation and inter-molecular motion on spectrum examined.
11	Alejandre, Tildesley, Chapela. J. Chem. Phy. 1995	MD simulation of orthobaric densities and surface tension of water.	SPC/E potential with full ewald summation used. Liq-vap. Equilibrium of water as a function of T.	Calculated surface tension (ST) and orthobaric density in good agreement with experimental results. SPC/E gives better orthobaric density than SPC and TIP4P. Polarizable model is not necessary for ST calculation. Long range dipole-dipole interaction important for ST.
12	Dang, Chang. J. Chem. Phy. 1997	MD study of water clusters, liquid and	Rigid 4-site polarizable model of water	For H <sub>2</sub> O hexamer, prism-like structure is predicted to have lowest energy and cage-like to have 2 <sup>nd</sup>

		liquid-vapor interface of water with many body potential	used. Various structural properties calculated. This allowed calculating the dipole moment of individual water molecules.	lowest. Dipole moment close to interface is similar to gas phase and away from interface to liquid bulk. Density profile shows interface is not sharp and has a thickness of 3.2 Å. $g_{OO}(r)$ deviates from experimental, due to O-O short range function chosen.
13	Maruyama et. al. Microscale thermophysical Engg. 1998	Liquid droplet in contact with a solid surface.	Liquid droplet and surrounding vapor – LJ. 3-layer harmonic molecule and 1-layer rigid molecule represent the solid surface.	$l-v$ and $s-s$ interaction LJ with variable energy scale parameter. $\cos\beta$ was well expressed by a linear function of the depth of integrated interaction potential of surface. Layered structure of droplet near surface explained by integrated interaction potential. 3-phase contact line in evaporation process was observed.

			Two surfaces at different T, evaporation on one and condensation on other.	
14	Bayazitoglu, Maruyama, Hos	Phase change studies with MD: A computer simulation	Algorithm and Code given. Truncated LJ used.	Code and algorithm given for MD simulation of an evaporating droplet. Discusses the nucleation process and size of critical nuclei.
15	Maruyama, Kimura RIKEN 1998	A MD simulation of a bubble nucleation on solid surface.	Liquid Ar on a 3-layer harmonic molecule solid surface. <i>l-s</i> interaction by LJ with variable energy scale parameter.	Equilibrium liquid with solid obtained first. Constant T surface is expanded to required Pr. And bubble nucleates on bottom surface. As wettability increases, minimum pressure approaches the 'Spinodal Line'. For very high wettability situation comes close to homogeneous nucleation.
16	Blomer,	MD simulation	Gas atoms:	Exchange of energy and

	Beylich. Surface science 1998	of energy accommodation of internal and translational DOF at gas- surface interface	right rotators. Surface atoms are in a T bath, Langevin equation used.	momentum during collision between diatomic gas molecules and solid surface. Strong coupling between trans. And rot. DOF for directly scattered molecules. Sticking coefficient dependent on KE and PE of incoming molecule. Molecules leaving surface after physisorption show the effect of rotational cooling at higher T.
17	Maruyama, Kimura ASME/JSME conf. 1999	A MD simulation of a bubble nucleation on solid surface.		Same as 15.
18	Maruyama, Kimura Th. Science & Engg. 1999	A study on thermal resistance over a solid-liquid interface by MD method	Quasi-steady non- equilibrium heat transfer simulation. Vapor	Energy flux through the system was calculated by controlling wall temperature using phantom method. T distribution shows jump over <i>s-l</i> interface. Thermal resistance was equivalent

			sandwiched in liquid layer, in contact with solid.	to 5~20 nm thickness of liquid sheet and strongly dependent on wettability. Thermal resistance increases sharply with decrease in wettability.
19	He, Shoji, Maruyama. ASME/JSME 1999	Numerical study of pool boiling for steady state and transient heating	Bisection model used and Boiling curves and temporal variation in $T_s$ calculated.	Macrolayer model suitable for high heat flux regime. Macrolayer thickness plays more important role on the transient boiling, results in agreement with experiments. Lower transient heating rate, results similar to steady state. CHF increases with increasing heating transient. Evaporation of macrolayer has a great effect on increasing CHF in transient heating.
20	Kinjo et. al. Computational Mat. Science 1999	Computer simulation of fluid phase change: vapor	Homogeneous nucleation from supersaturated	For nucleation LJ system and water were compared. For bubble formation one component and two component

		nucleation and bubble formation dynamics	vapor. Bubble formation in stretched liquid.	systems were compared.
21	Keblinski et. al. J. Chem. Phy. 2000	MD study of screening in ionic liquids	MD of molten and gaseous NaCl	In weakly coupled regime the spatial correlation between ions decay monotonically. Screening length = debye length. It decreases as ionic coupling increases. In strongly coupled regime spatial correlation between ions decay oscillatory. Here screening length increases as coupling increases. Transition from monoatomic to oscillatory screening occurs at the shortest possible screening length.
22	Kimura, Maruyama JSME-KSME 2000	MD simulation of heterogeneous nucleation of	Ar vapor and one layer of harmonic atoms as solid.	Nucleation rate, critical nucleus size and free energy of cluster formation were not much different than results of classical heterogeneous

		liquid droplet on solid surface.	Potential parameter varied to get different surface wettability	nucleation theory for smaller cooling rate or less wettability. Difference became large for higher cooling rate and increased surface wettability.
23	Maruyama et. al. IMECE 2001	MD Simulation of measurement of contact angle of water droplet on Pt surface	Water – SPC/E One layer of harmonic atoms in T bath for solid. H <sub>2</sub> O-Pt : Sphor (1989)	During spreading process, area of contact region between H <sub>2</sub> O-Pt expanded as $(t)^{1/3}$ For 256 molecules droplet, molecules spread forming a single monolayer. While for 856 molecules droplet, molecules form a thin secondary layer. Limiting values of advancing and receding contact angles were not reached even for a vertical surface.
24	Maruyama, Kimura Microscale thermophysical Engg. 2002	MD of heterogeneous nucleation of a liquid droplet on solid.	Ar vapor on one layer of solid molecules.	Same as 22 and 23



25	Maruyama, Kimura, Lu Th. Sc. & Engg 2002	Molecular scale aspect of liquid contact on a solid surface.	S-H and Z-P potential for H <sub>2</sub> O-Pt used. $\beta$ dependence on Pt surface structure is shown.	$\beta$ for LJ system seems to be scaled with p.e. parameter between <i>l-s</i> . Water layer on Pt. gives finite size $\beta$ on absorbed monolayer water film. $\beta$ determined by surface energy between this monolayer H <sub>2</sub> O and bulk liquid H <sub>2</sub> O.
26	Kebblinski et. al. J. Chem. Phy. 2003	Two regimes of thermal resistance at a liquid solid interface	NEMD used. Kapitza resistance observed. Strength of bonding between <i>l-s</i> affects thermal resistance.	Weak bonding (non-wetting liquid) resistance shows exponential behavior. Strong bonding (wetting liquid) resistance shows power law behavior. Nanocomposites or nanofluids characterized by weak atomic bonding at particle-matrix interface will exhibit high thermal resistance. Thermal resistance small for wetting liquids.
27	Kimura, Maruyama ASME-JSME	A MD simulation of water in contact	SPC/E for water. 3 layer harmonic	<i>l-v</i> interface initially semi-spherical and then gradually spreading. During spreading: $A_c \sim t^{1/3}$ (early

	2003	with Pt surface	atoms for Pt. H <sub>2</sub> O-Pt: SH & ZP Phantom mol. Below layer.	time), $A_c \sim t^{1/5}$ (later) For LJ, $A_c \sim \log(t)$ or $t^2$ Stronger H <sub>2</sub> O-Pt potential gives larger $\beta$ , because of repulsive effect of dense monolayer. $\beta$ was largest on fcc (100).
--	------	-----------------	--	--

## CHAPTER 3: METHODOLOGY

The basic assumption of continuum that the properties of material e.g. temperature does not change very fast with change in time and space breaks down at nano-scale. At nano-scale, we observe that the properties of materials change at the atomic scale and so the continuum approach can not be used to simulate these systems. No conventional equations or correlations are available to analyze the systems at micro and nano-scale. Experiments can be performed to study these systems but we can not do experiments over and over again because of the cost associated with these is very high. So the only feasible method to systematically study these phenomena occurring at molecular level is by way of numerical experiments.

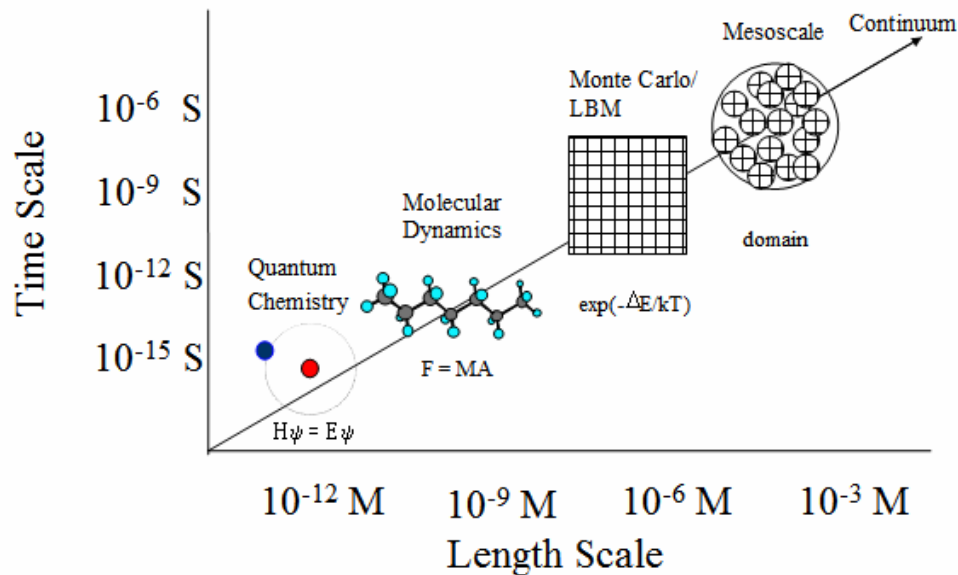


Figure 4: Simulation techniques for various length and time scales

Figure 4 [Smith G., 1999] shows different numerical methods that can be used at various length and time scales. At millimeter length scale the assumptions used to derive continuum level

equations are valid so we can use Navier-Stokes equations for fluid flow at this scale. Conventional Finite Element Modeling (FEM) or Computational Fluid Dynamics (CFD) numerical methods can be used to simulate the fluid flow and heat transfer at this scale. When the dimensions are of the order of few hundred micro-meters than also these conventional methods can be used with reasonable accuracy. As we move to sub-micrometer dimensions the assumptions used in the continuum models do not hold and we can not use the continuum models to appropriately model the systems with sub-micrometer length scales. At this scale *Monte Carlo* (MC) method or *Lattice Boltzmann Method* (LBM) numerical techniques can be used to accurately simulate the fluid flow and heat transfer. As we move to nano-scale length scales MC and LBM can not be used to simulate the atomic scale system. At this scale we should use a numerical technique which deals with individual atoms and *Molecular Dynamics Simulation* is a very good method to simulate the systems involving atomic size length scales. As the length scale decreases further and we deal with individual electrons *Quantum Chemistry* based methods e.g. *Quantum Molecular Dynamics* or *Density Functional Theory* methods can be used to model the systems.

Conventional FEM or CFD approach can not be used for this problem as these models break down at micro-scale when the mean free path and the system size become of same order. Molecular Dynamics (MD) simulation is becoming a very widely used simulation technique for numerical simulation at molecular level. MD is a computer simulation technique where the time evolution of a set of interacting atoms or molecules is followed by integrating their equations of motion. With this technique we can simulate the motion of molecules to gain a deeper understanding of complex physical and chemical reactions, fluid flow, heat transfer, phase

transformation and other physical phenomena that are driven by molecular interactions. Not only can we simulate motion of individual atoms or molecules in a fluid, but also the motion of a single large molecule consisting of many hundreds of atoms, e.g. protein or some other biomolecules. MD is a very powerful simulation technique and does not require the use of empirical sub-models for each physical process. Accuracy of MD simulation depends on the interatomic potential used to simulate the interactions between various atoms and finite difference scheme used to march in time. For a detailed overview of MD simulation Ercolessi [1997], Rapaport [2004] and Haile [1997] serve as excellent introductions to the molecular simulation technique.

### **3.1 Molecular Dynamics Simulation**

In molecular dynamics we follow the laws of classical mechanics and numerically solve Newton's equation of motion for each particle at every time step. The classical equation of motion for a simple atomic system can be written as:

$$m_i \ddot{r}_i = f_i = \sum_{\substack{j=1 \\ j \neq i}}^N f_{i,j} \quad (3.1)$$

Where  $m_i$  and  $r_i$  are mass and position vector of  $i^{th}$  atom,  $N$  is the total number of atoms in the simulation domain,  $f_{i,j}$  is the force applied on atom  $i$  by atom  $j$ , and  $f_i$  is the force acting on  $i^{th}$  atom due to interaction with other  $N-1$  atoms in the simulation domain. Since force is a vector quantity, so the sum in Eq. (3.1) is a vector sum of all the terms. So given an initial set of positions and velocities of all the particles in the simulation domain, the subsequent time evolution of the system can be completely determined. In more pictorial terms the atoms "move" in the simulation domain bumping into each other and using Newton's law we calculate the

acceleration of each particle using the force acting on it by other atoms in the system. The acceleration of each particle is then integrated numerically to calculate its velocity and new position at each time step. All other properties of the system e.g. potential energy, kinetic energy, temperature etc are calculated from the velocity and position of each particle. Figure 5 shows a flowchart of molecular dynamics algorithm.

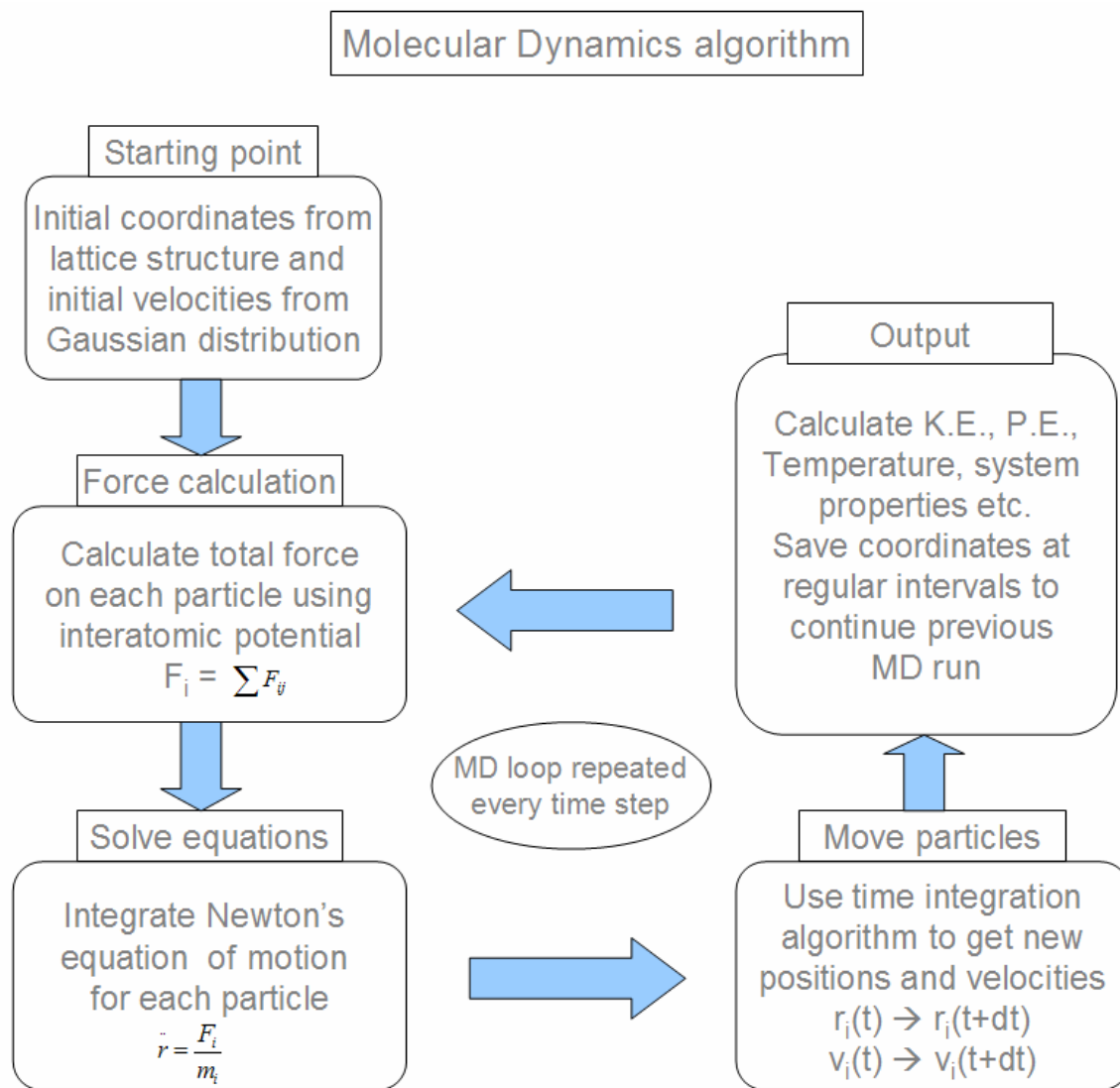


Figure 5: General flowchart of MD algorithm

Accuracy of a MD simulation is greatly affected by the choice of potential function used to simulate the interaction between atoms. The potential is a function  $u(r_1, \dots, r_N)$  of the positions of the nuclei, representing the potential energy of the system when the atoms are arranged in that specific configuration. This function is usually constructed from the *relative* positions of the atoms with respect to each other, rather than from the absolute positions. Forces on each atom are then derived as the gradient of the potential with respect to the atomic displacements:

$$f_i = -\nabla_{r_i} u(r_1, \dots, r_N) \quad (3.2)$$

Thus we can describe a model in terms of force or the potential energy. Since potential energy is a scalar quantity it is convenient to describe the model in terms of its potential energy. In this work liquid-liquid, liquid-solid and solid-solid molecules interaction e have considered. These interactions occur between silicon-silicon, silicon-oxygen (of silica), oxygen-oxygen, silicon-hydrogen and silicon-oxygen (of water molecule) atoms. These 5 kinds of interactions have been simulated with 3 different interatomic potentials, which will be mentioned later in this chapter. The electrostatic interaction between the charged atoms of water and silica has also been computed using wolf method.

The interaction potential used in a MD simulation can be non-bonded and bonded in nature. Most of non-bonded potentials are represented in terms of a pair potential, which means the interactions between the atoms is considered as one pair at a time. The simplest and most widely used pair-potential in MD simulation is Lennard-Jones [1924] or L-J potential. The L-J potential is a 12-6 potential which is attractive when the molecules are far apart and becomes strongly

repulsive when they come close together. L-J potential has a  $1/r^6$  attractive term which represents the attractive van der Waals interaction between atom at large distances and a  $1/r^{12}$  repulsive term which becomes dominant when atoms come close to each other this essentially represents the resistance to compression among atoms. For two atoms  $i$  and  $j$  the L-J pair potential is represented as:

$$\Phi_{LJ}(r) = 4\varepsilon \left[ \left( \frac{\sigma}{r} \right)^{12} - \left( \frac{\sigma}{r} \right)^6 \right] \quad (3.3)$$

Where  $r$  is the interatomic distance between a pair of atoms,  $\varepsilon$  is the energy constant (or well depth) and  $\sigma$  is the diameter of one of the atoms. The resulting potential is shown in Figure 6.

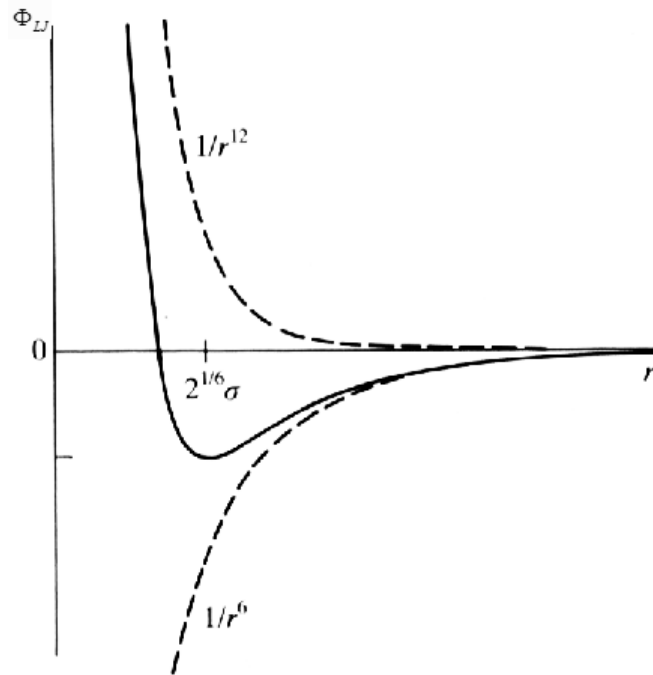


Figure 6: Potential energy of a particle in LJ model



The interaction pair potential is then used to calculate the force between the pair of atoms and force on an atom  $i$  is then calculated by summing the interactions over all other atoms in the system. The force is calculated as shown in Eq. 3.2. For L-J potential the interatomic force between two atoms is given by:

$$f_{LJ}(r) = \frac{\varepsilon}{r} \left[ 48 \left( \frac{\sigma}{r} \right)^{12} - 24 \left( \frac{\sigma}{r} \right)^6 \right] \quad (3.4)$$

The force calculation is the most time consuming step in MD simulation since force on each atom  $i$  by all other  $N-1$  atoms in the simulation domain is calculated. Moreover at each time step the force on each an every atom from all remaining atoms in the simulation domain has to be calculated. The force calculation grows as  $O(N^2)$  in MD simulation. In order to save some computation time, a cut-off radius  $r_{cut-off}$  is used in MD simulation and for atom  $i$  the interaction by atoms which fall outside a sphere of radius  $r_{cut-off}$  is neglected. The L-J potential with implementation of cut-off radius is represented as:

$$\begin{aligned} \phi(r) &= \phi_{LJ}(r) - \phi_{LJ}(r_c) & \text{if } r \leq r_c \\ \phi(r) &= 0 & \text{if } r > r_c \end{aligned} \quad (3.5)$$

Commonly used cut-off radius for LJ potential is  $2.5\sigma$  -  $3.2\sigma$  [Allen, 1987].

At every time step the force on every atom is calculated and then using Newton's law the acceleration of the particle is calculated. Then a time marching algorithm is used to calculate the velocity and new position of each atom from the acceleration. Verlet [1967] and predictor-corrector [Allen, 1987] algorithms are commonly used for marching in time in a MD simulation. Velocity verlet method is used to do the time marching in our MD code. The basic idea is to write one forward and one backward third-order expansion Taylor series expansion of the position  $r(t)$ :

$$\begin{aligned} \mathbf{r}(t + \Delta t) &= \mathbf{r}(t) + \mathbf{v}(t)\Delta t + (1/2)\mathbf{a}(t)\Delta t^2 + (1/6)\mathbf{b}(t)\Delta t^3 + O(\Delta t^4) \\ \mathbf{r}(t - \Delta t) &= \mathbf{r}(t) - \mathbf{v}(t)\Delta t + (1/2)\mathbf{a}(t)\Delta t^2 - (1/6)\mathbf{b}(t)\Delta t^3 + O(\Delta t^4) \end{aligned} \quad (3.6)$$

Where  $\mathbf{v}(t)$  is the velocity,  $\mathbf{a}(t)$  is the acceleration and  $\mathbf{b}(t)$  is the third derivative of  $\mathbf{r}$  with respect to  $t$ . Adding the two expressions we get:

$$\mathbf{r}(t + \Delta t) = 2\mathbf{r}(t) - \mathbf{r}(t - \Delta t) + \mathbf{a}(t)\Delta t^2 + O(\Delta t^4) \quad (3.7)$$

This is the basic form of the Verlet algorithm, in which first we calculate  $r(t+\Delta t)$  from  $r(t)$ ,  $r(t-\Delta t)$  and  $a(t)$  and then use  $r(t+\Delta t)$  and  $r(t-\Delta t)$  to calculate  $v(t)$ . Now we can calculate the velocities using the position as:

$$\mathbf{v}(t) = \frac{\mathbf{r}(t + \Delta t) - \mathbf{r}(t - \Delta t)}{2\Delta t}. \quad (3.8)$$

However, the error associated with velocity is order  $\Delta t^2$  unlike the error in position which is order  $\Delta t^4$ .

Periodic boundary condition (PBC) is used in almost all MD simulation codes where a wall is not encountered. The PBC acts in a way to simulate the bulk property of the system. In PBC each face of the cubic simulation domain acts as a mirror and there is a mirror system on the other side of the boundary. So every atom in the simulation domain actually represents infinite set of particles in the replicated systems. All these “image” particles move together but are represented by only a single atom in the actual simulation domain. Provided the interatomic forces are not long-range we can consider that an atom only interacts with its nearest atom or image in the periodic array. So every atom  $i$  in the simulation domain now interacts not only to the atoms  $j$  in the simulation domain but also to the images in the surrounding boxes. If an atom comes close to the boundary and then crosses it, it is re-inserted in the system from the opposite boundary with same velocity. So the PBC actually makes sure that the number density of atoms in simulation domain and the momentum of whole system is conserved. In MD code, the PBC is applied in the following way:

$$\begin{aligned}
 r_x &= r_x && \text{if } r_x < l_x \\
 r_x &= r_x - l_x && \text{if } r_x > l_x \\
 r_x &= r_x + l_x && \text{if } r_x < 0
 \end{aligned}
 \tag{3.9}$$

Where  $r_x$  is the x-coordinate of the atom  $i$ ,  $l_x$  is the length of the simulation domain in x-direction. It is assumed that one of the vertices of the simulation domain is the origin.

In a MD simulation the force calculation is the computationally most intensive step because we have to calculate forces on each atom  $i$  by all other atoms in the simulation domain. Even after using the cut-off radius we do not save a lot on computation time since for each atom  $i$  we have

to calculate  $r_{ij}$  for all other  $N-1$  atoms in the simulation domain and check if atom  $j$  lies inside or outside the cut-off radius. Other efficient algorithm called the *neighbor list* has been developed by Verlet [1967] which significantly reduces the computation time spent in force calculation. The basic principle of this algorithm is that we create a neighbor list for each atom  $i$  and calculate the force on  $i$  by only the atoms which lie in this neighbor list. This algorithm saves lot of computation time because this neighbor list is not updated at every step but is updated after few time steps, namely 10. So now  $r_{ij}$  is calculated new neighbors are checked in every 10 time steps.

Now in this interval of 10 or more time steps some of the atoms might move outside the cut-off radius or some new atoms might come in so in order to account for this movement, the neighbor list is generated using a slightly longer radius  $r_{list}$ . Where  $r_{list} = r_{cut-off} + \Delta r$ . Figure 7 shows the effect of  $r_{list}$  while generating the neighbor list.

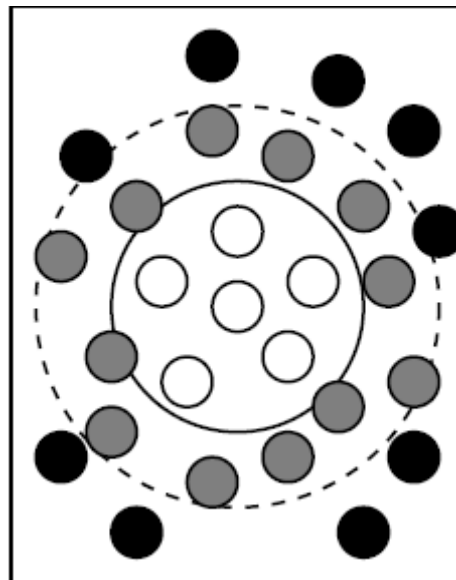


Figure 7: Neighbor-list construction with radius  $r_{list}$

## **3.2 Potential Functions used in Simulation**

In a conventional sense, MD uses interatomic potentials derived based on *ab initio* calculations. From these potentials the interaction force between atoms, the kinetic and potential energies of atoms are calculated. As a result the accuracy and validity of the MD simulation are dependent on the potential functions used. In order to accurately simulate the nanofluid system under consideration all possible atomic interactions have been considered. In this simulation interactions between Si-Si, Si-O, O-O, O-H and Si-H along with the coulombic interaction between charged particles are taken into account. This chapter discusses all the potential functions used in this work.

### **3.2.1 Interactions in Silica Nanoparticle**

The silica nanoparticle in this simulation consists of silicon and oxygen atoms arranged in  $\alpha$ -quartz structure. Although the nanoparticle as a whole does not carry any charge, but individual silicon and oxygen atoms carry positive and negative charges respectively. The condition for charge neutrality then becomes  $q_O = -1/2 * q_{Si}$ , where  $q$  is atomic charge. The van Beest–Kramer–van Santen (BKS) interatomic potential [van Beest et al, 1990, Kramer et al, 1991] is used in our simulation to model the Si-Si, Si-O and O-O interactions and calculate interatomic forces between atoms in the silica structure. It was shown by [van Beest et al, 1990] that for atomic charge of  $q_O = -1.2e$  and  $q_{Si} = +2.4e$ , the results from BKS potential agree well with *ab initio* calculations. The BKS potential represents the potential energy  $U_{ij}$  between atoms  $i$  and  $j$  as follows:

$$U_{i,j} = \frac{q_i q_j}{r_{i,j}} + A_{i,j} \exp(-b_{i,j} r_{i,j}) - \frac{c_{i,j}}{r_{i,j}^6} \quad (3.10)$$

Where  $r_{ij}$  is the interatomic distance,  $q$  is an atomic charge and  $A$ ,  $b$  and  $c$  are constants specified by the types of atoms  $i$  and  $j$  (silicon or oxygen) and are provided in Table 4. The BKS potential reproduces the static silica structure reasonably well. The simulated infrared spectrum agrees well with experimental spectrum at high frequencies but decreases at lower frequencies. The BKS potential is used by many researchers and is proven to be a sophisticated expression to derive the interaction between atoms in silica structure [Vladimir 1999, McGaughey and Kaviany 2004, Philippe and Rémi 1999].

Table 4: Force field parameters for silica nanoparticle

i,j	short range parameter			atomic charges
	$A_{ij}(\text{eV})$	$b_{ij}(\text{\AA}^{-1})$	$c_{ij}(\text{eV}\text{\AA}^6)$	
O-O	1388.773	2.7600	175.00	$q_{\text{O}}=-1.2$
Si-O	18003.7572	4.87318	133.5381	$q_{\text{Si}}=2.4$

### 3.2.2 Liquid-Liquid Interaction

Many effective pair potentials have been used to model interaction between water molecules in MD simulation, such as ST2 model [Stillinger, 1984], SPC model [Berendsen et al, 1981], TIPS model [Jorgensen, 1981] and TIPS2 [Jorgensen, 1982]. The SPC model proposed by Berendsen et al, was derived from a series of MD simulation and the parameters were derived to match the experimental density and vaporization energy of liquid water. The dipole moment calculated

from SPC (simple point charge) model is 2.27D, compared to 1.85D for the isolated water molecule. It gives a density of 0.98 gm/cm<sup>3</sup> at 300K and performs satisfactorily for most purposes. But the radial distribution function and diffusion coefficient needed some improvement and so Berendsen et al, [1987] reparametrized the SPC model to obtain correct energy and better matching density and called it SPC/E (extended simple point charge) model. The SPC/E model conformed better to experimentally measured properties of liquid water and so it is used in this simulation. SPC/E is a three site model for liquid water corresponding to one oxygen atom and two hydrogen atoms. Figure 8 shows the structure of SPC/E water molecules. Water molecule as a whole is neutrally charged but individual atoms carry certain charge.

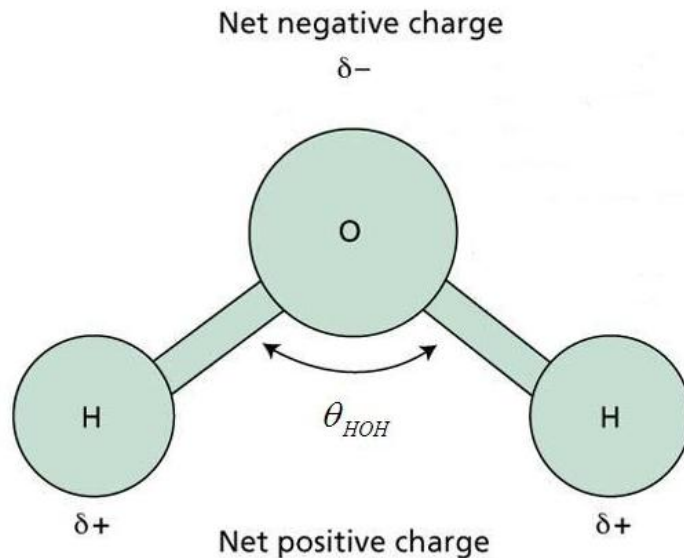


Figure 8: Structure of water molecule in SPC/E model

SPC/E model employs the water structure as bond length,  $r_{O-H} = 0.1nm$  and the angle  $\theta_{HOH} = 109.47^\circ$  with charges directly on oxygen and hydrogen atoms. It takes charge on oxygen and hydrogen atoms equal to  $\delta^- = -0.8476e$  and  $\delta^+ = +0.4238e$ , respectively. As one of the rigid

water molecule model, SPC/E adopted the higher permanent dipole moment of isolated water than the experimental value. The direct inclusion of the polarizability to the water models results in the many-body potential in effect, which improves the accuracy of SPC/E model. Since the SPC/E model has found many successful applications in modeling the thermal properties of liquid water in this study, we also use SPC/E model for the effective pair potential form for water. Here the potential energy  $U_{ij}$  is expressed as:

$$U_{ij}(R_1, R_2) = \varepsilon_{oo} \left[ \left( \frac{\sigma_{oo}}{R_{12}} \right)^{12} - \left( \frac{\sigma_{oo}}{R_{12}} \right)^6 \right] + \sum_i \sum_j \frac{q_i q_j}{r_{ij}} \quad (3.11)$$

here,  $R_{12}$  represents the distance of oxygen atoms,  $r_{ij}$  the distance between charges  $i$  on molecule 1 and charge  $j$  on molecule 2 ( $i$  and  $j$  are even for positive charges, odd for negative charges), and  $\sigma_{oo}$  and  $\varepsilon_{oo}$  are Lennard-Jones parameters taken from [Berendsen et al, 1987].

### 3.2.3 Solid-Liquid Interaction

The third important potential to establish is the interfacial potential between the silicon atom on the surface and the liquid molecules. Although some methods are available [Kimura and Maruyama, 2002] to decide the solid-liquid potential, they do not account for the interaction of the solid atoms with one another. Instead they employ L-J like potentials for the big molecules interacting with the whole wall. We have employed Si-H pair potential, a two-body KTS potential expression [Kohen et al, 1998] as follows:

$$U_{ij} = \alpha_{ij} (\beta_{ij} r_{ij}^{-p} - 1) \exp \left[ a_{ij} / (r_{ij} - b_{ij}) \right] \quad (3.12)$$

where,  $r$  is the distance between a pair of atoms,  $b$  is the cutoff distance of the two-body potentials,  $\alpha$ ,  $\beta$ ,  $p$  and  $a$  are fixed parameters chosen by Stillinger and Webber [1985].



### 3.2.4 Coulombic Interaction

Till now we have discussed various pair potential functions used in this simulation. These interactions are essentially short-ranged in nature, which means that the potential decreases quickly as the distance between a pair of atoms increases and we can use a cut-off radius to ignore the interactions with interatomic distance larger than the cut-off radius. Short-range interactions exclude a very important group of interactions involving electric charges and dipoles. In this system even though individual water molecules are electrically neutral but individual oxygen and hydrogen carry negative and positive charges respectively, similarly the silica nanoparticle as a whole does not carry any charge but oxygen and silicon atoms carry negative and positive charges respectively. The interactions between electric charges are long-ranged in nature, which means that the force between charges does not decay even at large distances, so it can not be truncated and the interactions over the whole simulation domain should be considered. The electronic interaction between charge-charge decays as  $r_{ij}^{-1}$  and the interaction between dipole-dipole decays as  $r_{ij}^{-3}$ . So these interactions do not decay fast even at large distances. A spherical truncation using a cut-off radius can not be done here because the resulting sphere around a given charge could be charged (i.e. sum of all charges in the spherical domain might not be zero). Also the charges moving in and out of this spherical domain would create artificial surface effects at  $r=r_c$ . The electronic interactions or coulombic interactions essentially require  $O(N^2)$  computational time. Even with modern high speed computers this high computational cost is a serious problem in MD simulations with thousands of atoms.

In this simulation an approximate method called *Wolf method* [Wolf et al, 1999] is used to

simulate the coulombic interactions between charged atoms. The Wolf method was conceptualized on the fact that ionic systems have a tendency to be locally charge neutral, .e. the ions arrange themselves in such a way that each charge is surrounded by neighboring charges of opposite sign, thereby creating a locally charge neutral zone. This kind of behavior is called “screening” of ions and is observed in molten salts, ionic gases, ionic solutions and metallic conductors. It has been shown both theoretically [Evjen, 1932] and numerically [Clarke et al, 1984, Woodcock, 1975, Wolf 1992] that the effective coulombic interaction in condensed systems are actually short-ranged. It has also been suggested that at long range there is almost complete cancellation of coulombic effects. Based on these findings, Wolf et al [1999] proposed an exact method for simulation of coulombic system by spherically truncated, pairwise  $1/r$  summation. Wolf method is suited for this simulation since there are no ions in the simulation domain, individual atoms carry certain charge but the molecules as a whole are locally charge neutral.

This method sums the total potential energy over all the atomic sites in the system and solves iteratively the self-consistent equations for the induced dipoles at each step of the molecular dynamics. Since we are using a truncated potential the following term is added to the total potential energy of the system to consider the effect of interaction between charges which are at an interatomic distance greater than the cut-off radius.

$$U_{pol} = -\frac{1}{2} \sum_k \mu_k E_k \quad (3.13)$$

Where,  $E_k$  is the electric field at the location of site  $k$  due to all the fixed charges in the system and  $\mu_k$  is the induced dipole moment vector at location  $k$ . The induced dipoles are determined by iteratively solving the equation

$$\mu_k = \alpha_k \left[ E_k - \sum_{k \neq l} T_{kl} \cdot \mu_l \right] \quad (3.14)$$

Here  $\alpha_k$  is the atomic polarizability assigned to site  $k$ , and  $T_{kl}$  is the dipole–dipole tensor. In the above approach, one needs to readjust the positions of the charges for each atom, and to assign atomic polarizability to each atom without changing the form of each potential expression. The electrostatic interactions between charges  $q_i$  and  $q_j$  are then modeled using the following approximation,

$$\frac{q_i q_j}{r_{i,j}} = \frac{q_i q_j \text{erf}(\alpha r_{i,j})}{r_{i,j}} \quad (3.15)$$

The advantage of the Wolf method over the traditional Ewald sum method [Allen, 1987] is that it can significantly reduce the required computational time. The Wolf method is essentially equivalent to ignoring the long range electrostatic interactions in the Ewald sum method. Even though Wolf method ignores the long-range interaction but it is successful because it forces the net charge to be zero in the spherical volume confined by the cut-off radius. The parameter  $\alpha$  in Eq. (3.15) provides the damping necessary to make the electrostatic interaction short range. Demontis et al [2001] propose a value of  $4/L$  for  $\alpha$ , where  $L$  is the length of simulation domain. They also show that this value gives good agreement with the Ewald sum method. For the current simulation, two constant values of 0.25 and 0.07 are chosen for silica and water respectively.

### **3.3 Generation of Nanoparticle**

In order to establish a reliable molecular dynamic model, a crystallographic-based coordinate system is necessary to get the position of each atom in the nanoparticle. It is well known that before building a lattice structure, the primitive vector should be obtained and a unit cell of certain crystal need to be setup firstly. Due to the high degree of symmetry present in the crystal solid, the positions of atoms in the unit cell will be used to pile up the bulk of the perfect crystal, and after applying certain geometrical and electrically neutral restriction, we can obtain the structure of a real nanoparticle.

As for the silica (quartz), the primitive vectors are written as [The  $\alpha$  quartz structure]

$$A_1 = \frac{a}{2}x - \frac{\sqrt{3}a}{2}y, A_2 = \frac{a}{2}x + \frac{\sqrt{3}a}{2}y, A_3 = cz \quad (3.17)$$

here,  $a=4.9134$ ,  $c=5.52$  are the length scale of silica unit cell. With these primitive vectors, the fractional coordinate of each atom can be translated to its Cartesian coordinate. By using the space group structure and atomic Wyckoff sites with face centering generators  $(x,y,z)$ ,  $(-y,x-y,z+2/3)$ ,  $(-x+y,-x,z+1/3)$ ,  $(y,x,-z)$ ,  $(x-y,-y,-z+1/3)$ ,  $(-x,-x+y,-z+2/3)$  together, we can generate the fractional coordinates of all atoms in the unit cell. After piling up in the three different directions, and applying certain geometrical and electrically neutral restriction, we established the coordinate system of silica nanoparticles with the diameter 1nm, 1.5nm and 2nm. Figure 9 shows the replication of a single unit cell of silica and then the final nanoparticle after removing the

atoms outside the specified diameter. Figure 10 shows the 1nm and 2nm diameter nanoparticles (not to scale).

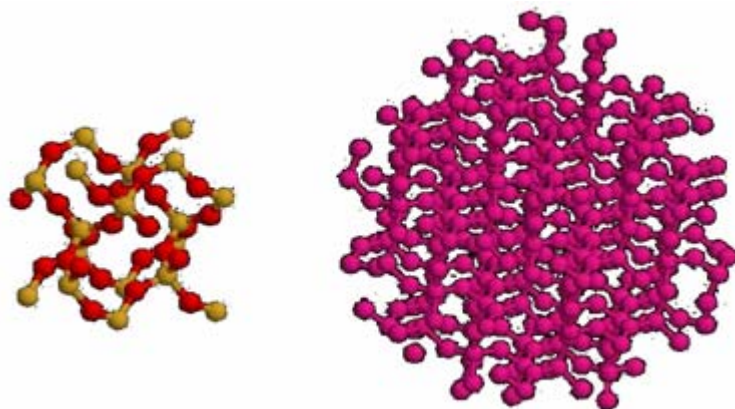


Figure 9: Generating the nanoparticles from Silica unit-cell

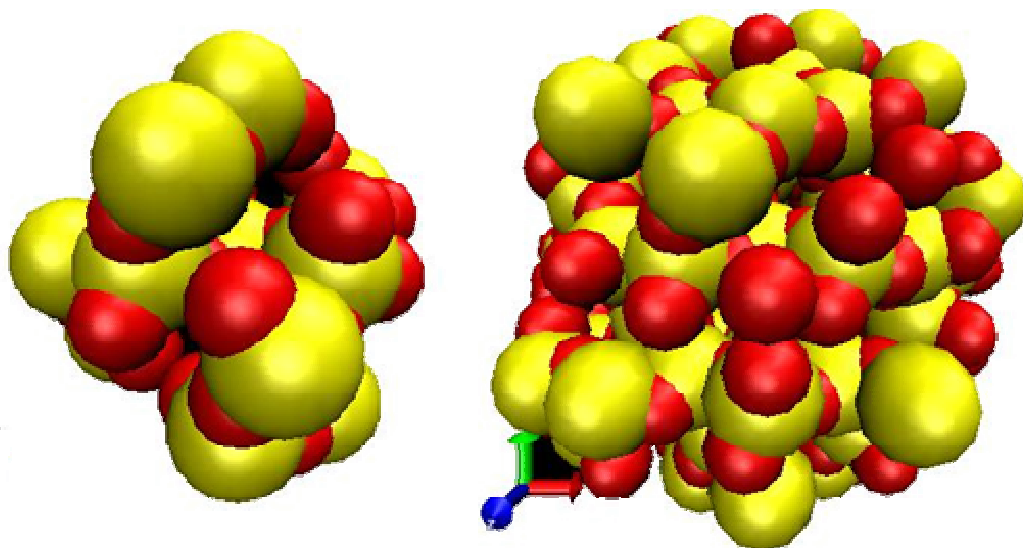


Figure 10: 1nm and 2nm diameter silica nanoparticles

### **3.4 Molecular Dynamics Simulation of Thermal Conductivity**

As mentioned in chapter two, thermal conductivity is obtained from molecular dynamics using either equilibrium (EMD) simulations (Green-Kubo equations) or from steady-state nonequilibrium (NEMD) simulations [Florain, 1997, Young et al, 1991]. In EMD, thermal conductivity is derived by simulating equilibrium conditions. In the range of linear response, thermal conductivity is related to the time autocorrelation function of the heat-flux operator according to the fluctuation-dissipation theorem. This relationship between correlation functions and transport coefficients are known as Green-Kubo relationships and for thermal conductivity it is given as follows:

$$\lambda = \frac{1}{3K_BVT^2} \int_0^{\infty} \langle q(0) \cdot q(t) \rangle dt \quad (3.18)$$

Here  $V$  is the volume of the simulation cell,  $t$  is time and  $q$  is the heat current, defined as

$$q = \frac{d}{dt} \sum_i r_i \cdot E_i \quad (3.19)$$

In Eq. (3.19), the summation is over the  $i$  particles in the system,  $r$  is the location of a particle and  $E$  is its total energy (kinetic and potential). For computational ease, Eq. (3.19) can also be written as

$$q = \sum_i E_i v_i + \frac{1}{2} \sum_{i,j} (F_{ij} \cdot v_i + N_{ij} \omega_i) r_{ij} \quad (3.20)$$

Here  $v$  is the velocity of a particle and  $r_{ij}$  and  $F_{ij}$  are the distance and force between particles  $i$  and  $j$ . The first term in eq. (3.20) corresponds to the contributions of convection, and the second term corresponds to conduction. The integrand of eq. (3.18) is the heat current autocorrelation function.

## CHAPTER 4: PARALLEL MOLECULAR DYNAMICS

Molecular dynamics simulations are valuable tools, but they are inherently computationally demanding. Every atom in a liquid simulation interacts with an average of fifty atoms at every time step and in a solid simulation it interacts with hundreds of atoms. Also to accurately model the interaction and collision dynamics and achieve the required simulation accuracy, the time step used in the simulations has to be very small, typically of the order of *femto-seconds* ( $10^{-15}$  s). Also as noted the study of heat transport at the surface of the nanoparticle requires models which are complex in nature, as a result this study requires efficient parallel coding on powerful computer architectures. One of the requirements of efficient parallel programming is load balancing. The computational load is proportional to the square of density. The density of silica is more than twice the density of water. Hence, the computational load in the solid region is four times that in liquid region. In order to overcome this problem a load balanced code was developed.

Here is a list of work done in the area of parallel molecular dynamics simulation. Srivastava and Barnard [1997] used lexical decomposition method to implement parallel MD code on shared-memory architecture. They used Brenner potential to simulate carbon nanotube (CNT) systems consisting of thousands of atoms on a parallel shared-memory supercomputer. One important feature of this code was that the  $O(N)$  cell-neighbor list method was implemented instead of  $O(N^2)$  serial neighbor list approach. Moldy [Refson K., 2000] is a general-purpose molecular dynamics simulation program. It is sufficiently flexible that it can be used to perform molecular dynamics simulation of solids and liquids with periodic boundary conditions. Moldy can be used

on a single processor as well as on a parallel platform. It is parallelized using parallel communications library such as MPI or BSP. The code is optimized for high performance in both serial and parallel cases. Moldy is highly portable and can be used on variety of computer hardware and operating systems, such as UNIX, Linux, Windows, Cray PVP (vector), Cray T3D, IBM SP2 and SGI Origin 2000 etc. It scales linearly with  $N$ , for non-coulombic systems and as  $N^{7/6}$  for coulombic systems. It has been also parallelized using the domain decomposition or space decomposition method. The system is specified at run time with a description file which can be a new system configuration file or a configuration file to restart the code from a previous run. Atomic interactions are simulated by pair-potentials and it can also simulate charged particles with coulombic interactions. Most common forms of potential functions are supported (Lennard-Jones, Buckingham, Born-Meyer, MCY) and the program is designed to make it very easy to add others. Short-ranged forces are handled using the link-cell method and the long-ranged coulombic forces by the Ewald sum. One shortcoming of Moldy is that only pair potentials are supported and many body interactions can not be simulated. New forms of pair-potential function are easily added, but bond-bending or 3-body forces will take rather more work.

NAMD (NAnoscale Molecular Dynamics) [Phillips et al, 2005] is a parallel molecular dynamics simulation package developed at the University of Illinois at Urbana-Champaign. It was first introduced by Nelson et al [1995] as a parallel molecular dynamics code enabling interactive simulation by linking to the visualization code VMD. NAMD is designed for high performance simulation of large biomolecular systems. It is highly scalable and can be scaled to tens of processors on small clusters to hundreds of processors on high end parallel platforms. It is noted



for its parallel efficiency and often used to simulate huge systems (millions of atoms). Developing modern high-performance software requires knowledge of parallel decomposition algorithms, communications libraries and the relative cost of accessing different levels of cache memory. The parallel decomposition strategy used by NAMD is the space decomposition method. It treats the simulation cell as a three-dimensional patchwork quilt consisting of smaller sub-cells, with each patch or sub-cell of sufficient size that only the 26 nearest-neighboring patches are involved in bonded, van der Waals, and short-range electrostatic interactions. This is ensured by taking the size of each sub-cell equal to or greater than the cut-off radius of the interatomic potential used in the simulation. In case of multiple interatomic potentials one should use the largest cut-off radius. This way the atoms in one sub-cell only interact with atoms in neighboring 8 sub-cells in 2-D and 26 sub-cells in 3-D simulation domain. When NAMD is run, patches are distributed as evenly as possible, keeping nearby patches on the same processor ensuring proper load-balancing. Each patch is responsible for calculating forces and integrating the equations of motion for the atoms it contains.

AMBER is a parallel molecular dynamics simulation program focused on molecular dynamics of proteins, nucleic acids, and carbohydrates. It evolved from a program that was developed to do Assisted Model Building and Energy Refinement (AMBER) calculations. Amber is also a family of force fields for molecular dynamics of biomolecules, and AMBER molecular dynamics simulation package implements these force fields to simulate various biomolecules. AMBER is also highly portable code and can be used on various platforms. It is parallelized using the MPI to communicate among processors. It is parallelized using the atom decomposition method. At each time step, each processor computes a portion of the potential energy and corresponding

gradients. The force vectors are then summed, so that each processor gets the full force vector components for its “owned” atoms. Each processor then does the time integration and updates the velocity and position of its "owned" atoms. Each processor has a "global" and a "local" position array, so all processors know the positions of all atoms.

Several techniques have been proposed by various researchers for parallelizing molecular dynamics code efficiently [Flincham, 1987, Gupta, 1992]. There are two basic methods proposed to parallelize short-ranged MD computations, *atom decomposition* and *special decomposition* method. These methods differ in the way they divide the atoms among various processors. All other proposed algorithms have been variations on these two methods. Plimpton [1995] proposed another method called *force decomposition* method which is a variation of the space decomposition method. All three methods scale well for small clusters but for large number of processors the communication cost associated with atom decomposition method increases faster compared to other two methods. Main aim while parallelizing a MD code is to divide the neighbor list generation, force calculation and time integration of equations of motion (almost) equally among all processors. One way to divide these computations is to divide all the atoms in simulation domain into sub-groups which consist of equal number of atoms and then assign these sub-groups to each processor. Each processor computes force on atoms in its sub-group no matter where they move in the simulation domain. This decomposition is analogous to Lagrangian gridding in fluid simulations where the grid cells move with the fluid (atoms in MD). In contrast, the other method divides the simulation domain into sub-domain and assigns these sub-domain to each processor. So each processor is assigned a portion of the simulation domain and hence the atoms contained in this sub-domain. Each processor computes the forces only on

the atoms residing in its assigned sub-domain at that time-step. As the simulation progresses the atoms move from one sub-domain to another and the processors exchange these particles. This method is analogous to the Eulerian gridding for fluid simulation where the grid remains fixed and fluid (atoms in MD) move through it. Using these two methods various other methods have been proposed to parallelize MD codes based on different parallel architectures, e.g. shared memory or divided memory or vector computers.

#### **4.1 Atom decomposition algorithm**

In this method for  $P$  processors the  $N$  atoms are divided into sub-groups of  $N/P$  atoms at the beginning of the simulation and assigned to each processor. The atoms in one sub-group can be anywhere in the simulation domain and need not have any special relation with each other. Here  $N$  may or may not be a multiple of  $P$ , if  $N$  is a multiple of  $P$  then we will get equal number of atoms assigned to each processor otherwise  $P-1$  processors will be assigned equal number of atoms and the  $P^{\text{th}}$  processor will have different number of atoms assigned to it. For simplicity, we will assume here that  $N$  is a multiple of  $P$  and each processor is assigned  $N/P$  atoms. Each processor will generate the neighbor list, compute forces and does time integration on only its assigned  $N/P$  atoms, no matter where they move in the simulation domain. At the end of the time-step each processor calculates the total potential energy and kinetic energy of its assigned atoms and sends it to the parent node using the `mpi_send()` MPI communication operation, which receives the individual potential and kinetic energy from each processor using the `mpi_recv()` MPI operation and then sums them to calculate the total potential energy and total kinetic energy of the whole simulation domain. Each processor updates the global position

matrix at the end of the time-step with a one-to-all *bcast()* MPI communication operation. This updated global position matrix is used to calculate the force on particles in the next time-step.

The algorithm for atom decomposition method as used in current work is shown in Figure 11.

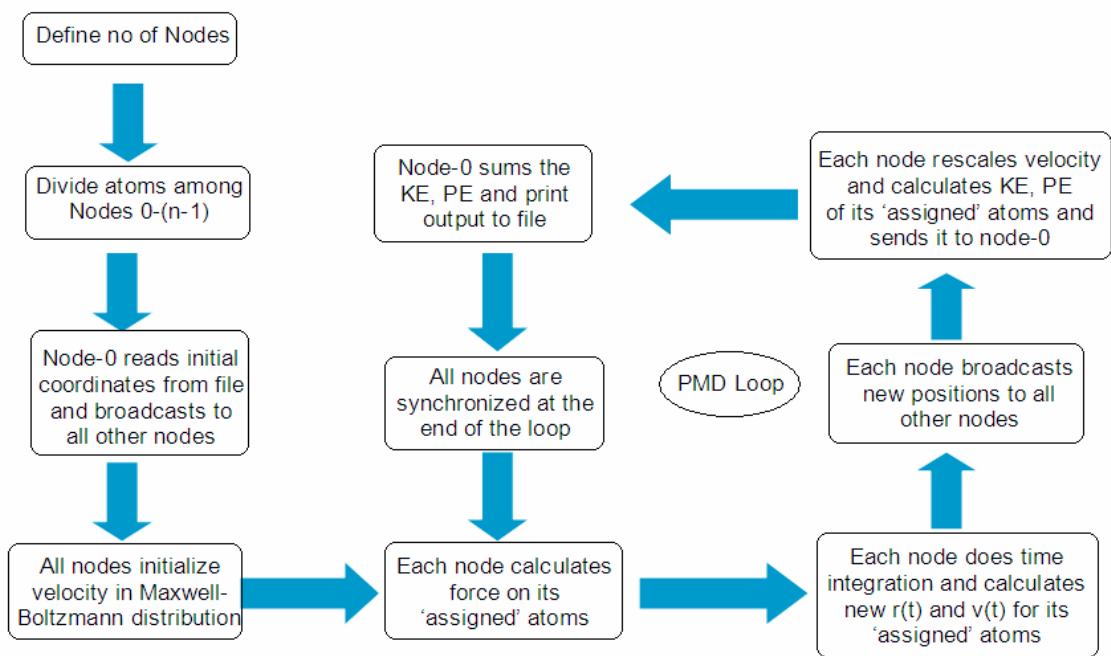


Figure 11: Flowchart of parallel molecular dynamics code

The cost of communication is typically quantified by the number of messages and total volume of data send and received among processors. The cost of communication associated with the broadcast operation increases as the number of processors increase. The method used to parallelize this code is the *atom decomposition* method. Atom decomposition method is also called replicated-data method [Smith, 1991] because identical copies of atom information e.g. coordinate, velocity are stored on all processors.

## **4.2 Spatial decomposition method**

As mentioned earlier in this method the simulation domain is subdivided into small 3D sub-domains, one for each processor. This method is called special decomposition or space decomposition method. At each time-step the atoms residing in the sub-domain are assigned to a processor which generates the neighbor list, computes forces on these atoms and updates their positions and velocities. While calculating forces on the atoms in one sub-domain the neighboring atoms can reside in the same sub-domain as well as the neighboring 26 sub-domains in 3-D simulation and in neighboring 8 sub-domains in 2-D simulation. So each processor has to have the coordinates of some atoms in neighboring sub-domains also to do the force calculation. Each processor keeps the coordinates of atoms in its assigned sub-domain and of atoms which are within the cut-off radius from each boundary in the neighboring sub-domains. At the end of each time-step each processor calculates the updated positions of atoms in its sub-domain and in this process some atoms which were near the boundary of the sub-domain might move to a neighboring sub-domain. So before starting a new MD time-step we have to look for those atoms which migrate to neighboring sub-domains and transfer their data e.g. position, velocity and charge etc to the new processor where it migrates. This process adds to the communication in space-decomposition method. We have to communicate the data associated with migrated atom from one processor to another. But since it is a one-to-one communication it does not add high communication cost. Also at the end of each time step each processor calculates the total potential energy and total kinetic energy of its assigned sub-domain and sends them to the parent node which receives it and sums it to calculate the total potential energy, total kinetic energy and total energy of whole simulation domain and prints the output to a file. The total energy data is

also used to check the energy conservation of the system. This process of communicating kinetic and potential energy from each node to the parent node also adds to the communication cost. But this communication process is also one-to-one communication (child node – parent node). Since all communications in the space decomposition method are one-to-one in nature it does not add huge communication overhead to the parallel code. This method scales almost linearly with increasing the number of processors and is preferred for huge parallel architectures. But keeping track of the migrating atoms from one sub-domain to another is a complicated process and can add to the complexity of the parallel code.

In this simulation thousands of atoms are being simulated using multiple complicated inter-atomic potentials. Since we are dealing with solid and liquid species the density is higher which means there will be hundreds of neighbors of each atom thereby increasing the total number of interactions to be simulated at each time-step. It is because of these reasons a parallel code was developed. As mentioned earlier in space decomposition method we have to keep track of the atoms migrating from one sub-domain to another at each time step, which is very complicated and adds communication cost if we have thousands of atoms so the algorithm used to parallelize this code is *atom decomposition* or *particle decomposition* method. Several groups have developed this method over the past few years. Sato *et al* [1992] describe the load balancing advantages and communication costs associated with this method and also predict the lack of scalability of this method for large number of processors because of large increase in cost of communication with increasing number of processors. Brown *et al* [1993, 1994] show the development of both atom decomposition and space decomposition methods. They used MD simulations for polymer modeling and the inherent density variation in their system made atom

decomposition method attractive. Kalia *et al* [1993] also developed both space decomposition and atom decomposition methods and used space decomposition for large number of processors, but for smaller number of processors both methods worked equally well. Plimpton [1995] reviews both atom decomposition and space decomposition methods in his paper and also proposes a new method called *force decomposition*. This method combines the load balancing capability of atom decomposition and scalability of space decomposition. In order to efficiently do load balancing of our varying density system we have used atom decomposition method to parallelize our code. We used 4 processors for each run in order to keep the communication cost low.

To develop a load balanced code the balancing of average number density for each processor for the life of the simulation was pursued. Since we are dealing with molecules and not individual atoms in this simulation this further complicates the problem because atom decomposition method divides individual atoms among different processors and not molecules. The atoms should be divided in such a way that all the atoms corresponding to a particular molecule should be handled by the same processor e.g. all three atoms of a particular water molecule should be processed by one processor. If different atoms of one molecule would end up with different processors this could result in breaking of bonds. As a result a run-time decomposition of atoms was not possible because of variety of atoms and molecules present in the simulations. The atoms were “manually” divided before the start of simulation to maintain equal loading on each processor and were kept same for the simulation time.

This atom decomposition technique solved the problem of load balancing but still a challenge lies to successfully implement the model. Since the atoms assigned to a processor can be anywhere in the simulation domain, its neighboring atoms can reside anywhere in the simulation domain and hence they can be assigned to different processors. At each time step the interaction forces are calculated between the atoms and for this coordinates of all the neighboring atoms are required by each processor at every time step. This complication was handled by using a *global* and a *local* list of coordinates. Each processor has a list of coordinates of all the atoms assigned to it (local) and a global list which consists of coordinates of all the atoms in simulation domain. Each processor makes use of the global list to create a verlet neighbor list for each atom, this neighbor list is renewed every few time steps. The interatomic forces on the atoms are calculated by each processor using this neighbor list on the atoms allocated to it. Since the coulombic interactions are long range the global coordinate list is used to calculate the electronic forces using the wolf method. Quaternian approach is used to take into account of rotation of water molecules. Each processor calculates the forces on atoms allocated to it and integrates to get new coordinates, then the global list is updated using efficient one-to-all broadcasting function “`mpi_bcast( )`”. It is because of this one-to-all communication at each timestep that the cost of communication is higher in the atom decomposition method compared to other decomposition techniques.

The cost in this approach is not the complicated coding, but the communication at every time-step, which involves each atom in the simulation domain. This suggests that the cost of communication is directly related to the number of atoms  $N$  in the simulation. Also, as we increase number of processors the computation cost per processor decreases but communication



cost increases. So this technique can not be used with large number of processors. In order to achieve both load balancing and scalability the force decomposition method can be used.

As noted, lot of work has been done in the area of heat transport study of nanofluids, modeling of nanofluids and parallel molecular dynamics simulation. However, the modeling of nanofluids with a large number of atoms and with sophisticated potentials has not been attempted before. The present work represents an initial step towards the large scale modeling of heat transport in nanofluids.

### **4.3 Simulation Procedure**

In the first case the simulation domain consists of 5851 water molecules and a 2nm silica nanoparticle consisting of 318 atoms in a cube of side length of 5.94 nm. In the second case the simulation domain consists of 845 water molecules and a 1nm silica nanoparticle consisting of 45 atoms in a cube of side length of 2.97nm. Number of water molecules is chosen such that the volume concentration of this system is around 2%. The silica nanoparticle is located at the center of domain, thus the interface between the solid and the liquid is around at  $r=1\text{nm}$  in first case and  $r=0.5\text{nm}$  in second. Periodic boundary condition is applied in all three directions. The simulation domain is initialized by surrounding the silica nanoparticle with water molecules in an fcc lattice. Water molecules are distributed in fcc lattice instead of random distribution in order to get a better distribution and faster equilibration.

The trajectories of all the atoms are determined by integrating the equation of motion according to the velocity verlet algorithm. Velocity rescaling is used at every 10 time steps to achieve temperature control. A time step of 1fs is used to ensure energy conservation, and the verlet neighbor list is employed in the simulation. The neighbor list is renewed every 100 steps. Green-Kubo relation is used to calculate the thermal conductivity of the simulated system.

## CHAPTER 5: RESULTS AND DISCUSSION

As mentioned in previous chapter, atomic scale simulation was used to simulate the motion and interaction of atoms. Molecular dynamics computations provide coordinates, velocities and forces of every atom at each MD time-step. Using the coordinates, velocities and forces, various transport coefficients of the system and also the motion of atoms can be calculated that give insight into the system behavior. A molecular visualization program *Visual Molecular Dynamics* (VMD), developed by the *Theoretical and Computational Biophysics group* at University of Illinois at Urbana-Champaign was used to visualize the motion of atoms. Visualization of atomic motion helps understand the output data and results better.

### **5.1 Lattice Vibration of the Nanoparticle**

Molecular dynamics simulation allows us to observe the motion of each particle in the simulation domain at every time step. The liquid molecules are free to move anywhere in the simulation domain but since the atoms in solid nanoparticle are bonded they can only vibrate about their mean position. The images and movies of atomic motion created using the VMD program helps in better understanding of the system dynamics. Since the atoms in silica nanoparticle are bonded and can not move randomly. It was observed that the atoms in silica nanoparticle were moving back and forth about their mean position. The atoms in nanoparticle move faster as the system temperature is increased. The motion of atoms in nanoparticle suggests that with all the interactions (Si-Si, Si-O, O-O, Si-H) described above, the lattice vibration of atoms in silica nanoparticle is induced. The lattice vibrations of the nanoparticles grow with increasing

temperature of the system. Motion of water molecules was also observed. It was observed that the liquid molecules were randomly moving in the simulation domain and they lost all the information of their initial coordinates as the simulation progressed. It was observed that when the system enters stable state, the water molecules far away from the nanoparticle move faster than the ones close to it. This is because the water molecules away from the nanoparticle interact less as compared to the water molecules close to the nanoparticle surface. The lattice vibrations of silica nanoparticle play a major role in enhancing the thermal conductivity of nanofluid. The lattice vibration of silica nanoparticle shows that the nature of heat transport in nanoparticle is phononic or ballistic transport and not diffusive. This was also suggested by Koblinski et al [2002] that the nature of heat transport in nano-structures is ballistic or fast diffusive phonon transport. It was also suggested that if the phonons initiated from one nanoparticle can persist in the liquid and get transmitted to another nanoparticle, this will greatly enhance the heat transfer in nanofluids.

## **5.2 Density Profile near the Interface**

Formation of an electric double layer around the nanoparticles has been predicted as a plausible reason for enhanced heat transport between liquid and nanoparticle. It is well known that the ions on nanoparticle surface can attract water molecules near it and the electrical double layer may be established due to the electrostatic interaction. Similar effect is observed from the density profiles obtained from the present simulation. Figure 12 shows the density profile for two nanoparticles. Initially, the solid and liquid are distributed in their respective areas, and the density in these areas is approximately constant. 50ps later, the density of silica decreases, while

that of the water increases at the solid-liquid interface. As the simulation evolves silica nanoparticle attracts more liquid particles, and the liquid density near the interface continues to increase. Two types of interactions are being calculated at the solid-liquid interface. One is the KTS interatomic potential between Si-H and other is the coulombic interaction between atoms with charges. Although the system as a whole is neutrally charged but individual atoms carry certain charges. In water, oxygen and hydrogen atoms carry negative and positive charges respectively. In silica nanoparticle, oxygen and silicon atoms carry negative and positive charges respectively. At smaller distances the KTS potential gives attractive force to water molecules and increases density of water near the nanoparticle, and due to the density gradient more water molecules are attracted towards the nanoparticle.

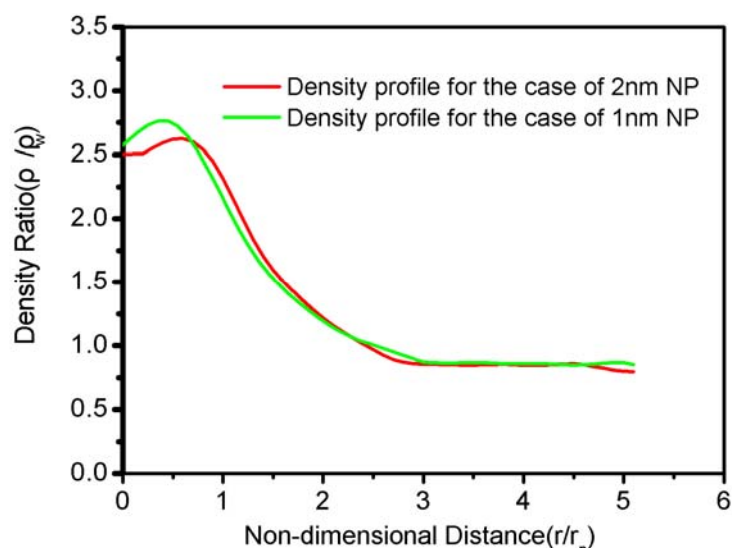


Figure 12: Smoothed density profiles of water for 1nm and 2nm nanoparticle at T=300K

The VMD program was used to generate images of positions of water molecules at various time steps. It was observed that as the simulation time increases the density of water molecules close to the nanoparticle surface increases and the density of water molecules decreases far away from

the solid-liquid interface. To clearly observe this phenomenon water molecules in a radius of  $\Delta r=0.5nm$  close to the interface and in a layer  $r-(r+\Delta r)=2.5-3.0nm$  were plotted. It was observed that the water molecules in the layer close to solid-liquid interface were densely packed compared to the atoms further away from the nanoparticle. The liquid molecules at the solid-liquid interface were arranged in a loosely packed structure, forming a liquid layer or hydration layer at the interface. Figure 13 shows the increased density of water molecules close to the surface of nanoparticle compared to far away. For clarity the water molecules are shown as a single atom at the center of mass.

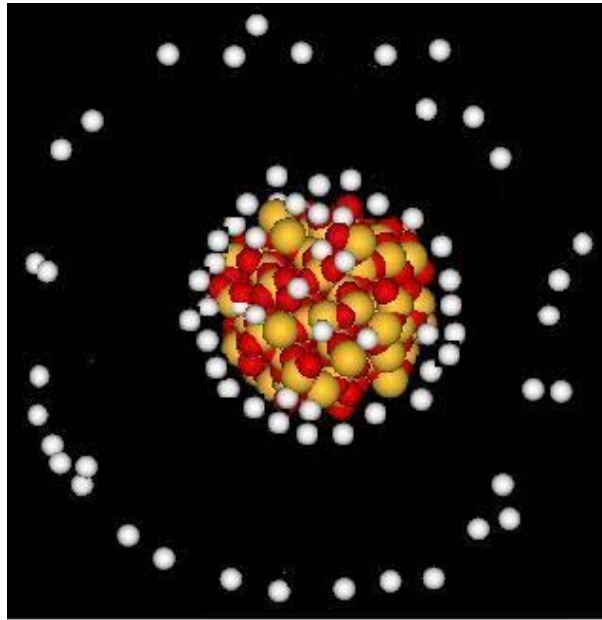


Figure 13: Density of water molecules higher close to the surface compared to far away

The liquid layer at the solid-liquid interface combined with the phononic nature of heat transport in nanoparticle is the two main mechanisms for thermal conductivity enhancement in nanofluids. The phonons initiated from one nanoparticle can now travel further in the liquid due to the ordered layer at the interface and can be transmitted to another nanoparticle. Although Brownian

motion of particles alone can not be accounted for the thermal conductivity enhancement of nanofluids, but the random motion of the nanoparticles will also help the phonons to be transmitted from one nanoparticle to another.

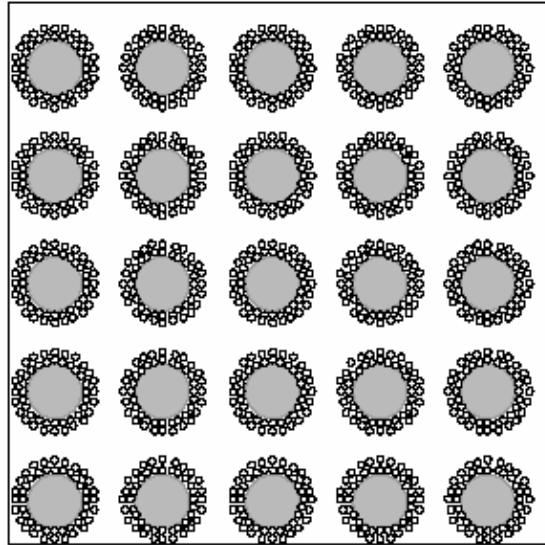


Figure 14: Schematic nanoparticle surrounded by liquid layer [Yu and Choi, 2003]

Yu and Choi [2003] have also observed in their experiments the formation of double layer in their experiments. Figure 14 shows the schematic of nanofluid structure consisting of nanoparticles, bulk liquid, and nano-layer at solid/liquid interface. They have shown that typical interfacial width is only of the order of a few atomic distances, i.e. 1nm. While in our simulation we observe the interfacial width is up to 2nm. The width of the interfacial liquid layer is highly dependent on the solid-liquid interactions. For weak solid-liquid interaction e.g. a non-wetting liquid either there will be no interfacial layer or if it is there then it will be very small, while for a strong solid-liquid interaction e.g. wetting liquid there will be a thick interfacial layer. So, this

discrepancy may be attributed to the potentials used in this simulation and the actual charges of the particles in the experiment.

### **5.3 Heat Current Autocorrelation Function**

The thermal conductivity of the simulated system has been calculated using the Green-Kubo relationships. The heat current autocorrelation function was calculated for all the components of heat flux vector. Autocorrelation is a mathematical tool often used in signal processing to analyze functions in time domain or frequency domain. Autocorrelation is the cross-correlation of a function with itself e.g. heat current,  $q(t)$ . The green-Kubo relations give a mathematical expression for thermal conductivity in terms of the time integral of heat current autocorrelation function. The heat current autocorrelation function (HCAF) was plotted for water, nanoparticle and the nanofluid and following observations were made. The heat current autocorrelation function is a cross-correlation of heat current at time  $t$ ,  $q(t)$  to heat current at time  $0$ ,  $q(0)$ . The HCAF starts at value, 1 and then slowly decays as the simulation progresses. HCAF starts at maximum value 1, since at  $t=0$ , we take the cross-correlation of  $q(0)$  with  $q(0)$ . The two values being perfectly correlated, give a maximum value to the HCAF. As simulation progresses the atoms move randomly in the simulation domain and loose information about their initial condition and the heat current at time  $t$  becomes less and less correlated to the initial value and decays. The autocorrelation for water molecules show an oscillatory behavior to convergence unlike the monotonously decreasing behavior shown by Koblinski et al [2002]. Their simulation showed monotonously decreasing behavior probably because they used L-J potential for both



solid and liquid. In our simulation the silica nanoparticle and also the nanofluids heat current autocorrelation show oscillatory behavior due to the lattice vibration of the particle.

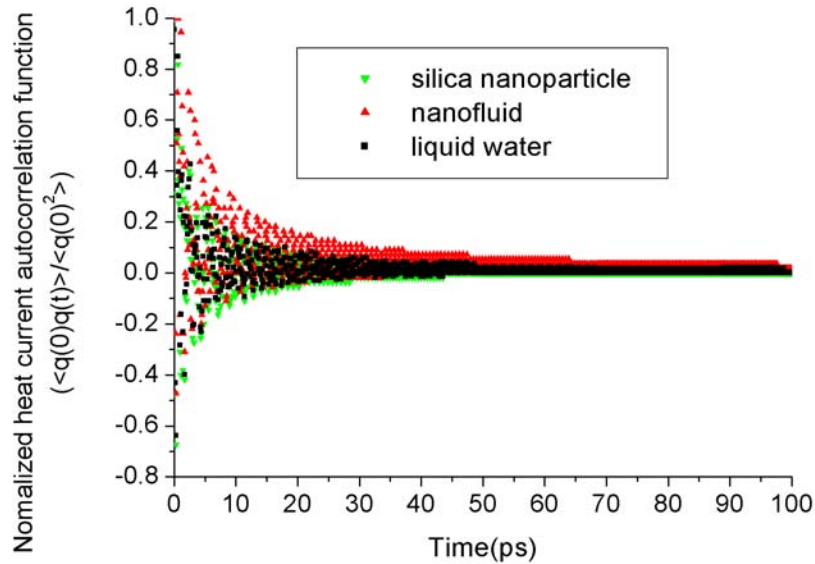


Figure 15: Heat current autocorrelation function

Since the number of water molecules used in the simulation is very large, the convergence takes more time for water molecules compared to the lattice system of silica nanoparticle. Figure 15 shows the heat current autocorrelation function for water, nanoparticle and the nanofluid.

#### **5.4 Thermal Conductivity Enhancement**

MD simulation of pure water was done to calculate the thermal conductivity of pure water and to validate the MD code. 256 water molecules were modeled using the SPC/E model in a cubic simulation domain of 1nm length. Thermal conductivity of liquid water was also calculated using

Green-Kubo correlations at three different temperatures. Thermal conductivity of pure water was 0.665 W/mK, 0.679 W/mK and 0.685 W/mK at 300K, 315K and 325K temperatures, respectively. At 300K the calculated thermal conductivity of liquid water is around 0.665 W/mK, which is larger than the experimental value (0.61 W/mK), but is still comparable with the simulation value (0.67 W/mK) provided by Bertolini and Tani [1997], this comparison also validates our MD code. Figure 16 shows the calculated thermal conductivity of silica nanoparticle, liquid water and the nanofluid. The simulated thermal conductivity for the silica nanoparticle is around 7.21 W/mK, and this value is less than the results, 8.2 W/mK for  $\alpha$ -directions provided by McGaughey and Kaviany [2004]. This nonconformity is due to the fact that the simulation done by McGaughey was performed for bulk silica, while the thermal conductivity in our simulation is calculated for a silica nanoparticle of 2 nm in the presence of liquid water.

Thermal conductivities of water and 3 nanofluids at various temperatures are given in Table 5. At 300 K 2nm nanofluid gives 23.31% higher thermal conductivity than the simulated value for water and 34% higher compared with the experimental thermal conductivity of water. The 1.5nm nanofluid at 300K shows 24.21% thermal conductivity enhancement compared to simulated value for water and the 1nm nanofluid at 300 K shows 26.92% increase in thermal conductivity compared to simulated value for water. Although there are few experimental results of thermal conductivity for the silica-water nanofluid, the simulated value is still much larger than obtained from the Hamilton and Crosser theory (8.1%). However, the simulated value of the thermal conductivity for the silica-water system is still much less than those predicted from the correlations obtained by other authors. This is because almost all correlations were based on at

least two mechanisms, for example, Brownian motion of nanoparticles and clustering among nanoparticles and in this simulation the Brownian motion and nanoparticle clustering is not considered. Even though these mechanisms are not considered in the current work, the preliminary results for the silica-water nanofluid obtained from the molecular dynamic simulation are still exciting.

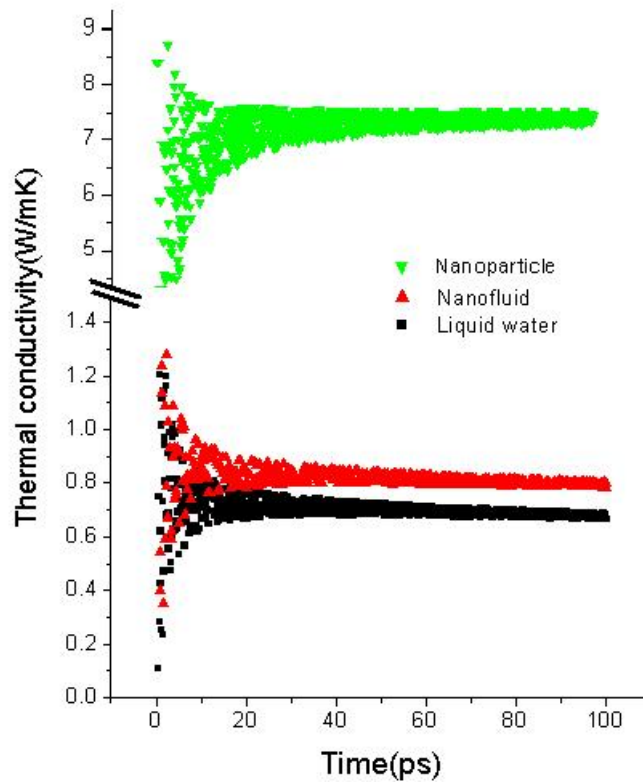


Figure 16: Thermal conductivity of water, nanoparticle and nanofluid at 300K

Thermal conductivity was calculated at various time steps and plotted over the simulated time to see the convergence as time progresses. Thermal conductivity of 1nm and 2nm nanofluids were plotted to see the effect of nanoparticle size on effective thermal conductivity of nanofluid. Figure 17 shows the thermal conductivity of water and effective thermal conductivity ( $k_{eff}/k_w$ ) of 1nm and 2nm nanofluid at 300K. Thermal conductivity of 1nm nanofluid is more than 3% higher

compared to that of 2nm nanofluid at all temperatures. The 1nm nanofluid gives more enhancements compared to 2nm because of higher surface area to volume ratio there are more interactions going on at the solid-liquid interface of 1nm particle than at 2nm particle. It can also be seen in Figure 17 that the extent of hydration layer was more for smaller size nanoparticle.

Table 5: Calculated thermal conductivity of 3 nanofluids at various temperatures

Temp	Water	1nm	% inc	1.5nm	%inc	2nm	%inc
	(W/mK)	(W/mK)		(W/mK)		(W/mK)	
300K	0.665	0.844	26.92	0.826	24.21	0.82	23.31
315K	0.679	0.862	26.95	0.8434	24.21	0.8374	23.32
325K	0.685	0.87	27.01	0.851	24.23	0.845	23.36

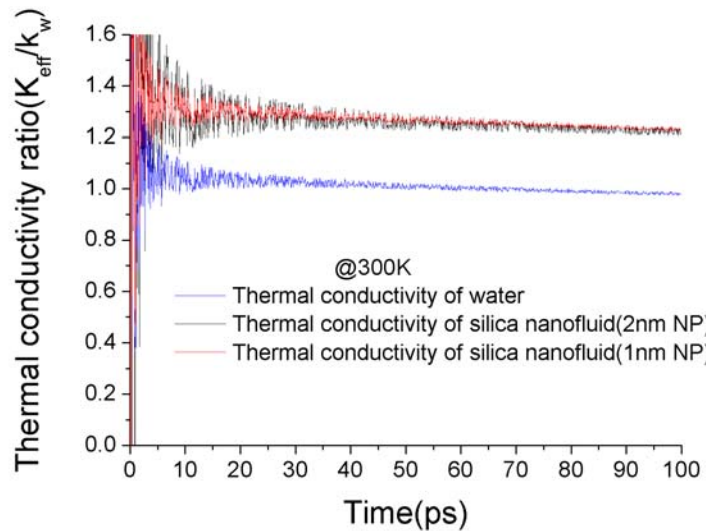


Figure 17: Thermal conductivity of 1nm and 2nm nanofluid and pure water at T=300K

In order to design better heat transfer devices involving the use of nanotechnology we need to understand the basic heat transport phenomenon at nano-scale. It is now well known that liquid molecules form an ordered layer on the solid-liquid interface and it has been postulated [Yu et al, 2000] that this ordered layer of liquid molecules help increase the thermal conductivity of nanofluid, because now phonons originating from the nanoparticle can travel further in the liquid and help the transport of heat. In this work we're considering interaction between solid nanosilica and liquid water molecules and the interactions between the two are modeled using the KTS model which provides a strong interaction hence a weak interfacial resistance. Yu and Choi [2003] have also postulated that the nanolayer formed on the solid-liquid interface helps augmentation of the thermal conductivity and solid-liquid contact resistance is not dominant at the solid-liquid interface of particle-in-liquid suspensions. So we conclude that the two most important mechanisms affecting the heat transport in silica nanofluid are liquid layering on the solid-liquid interface combined with phononic heat transport of nanosilica.

## CHAPTER 6: CONCLUSION

In this work, a parallel molecular dynamic simulation on the nanofluids consisting of one 1nm, 1.5nm and 2nm silica ( $\alpha$ -quartz) nanoparticle surrounded by water molecules has been performed. Both the short-range and long-range interactions have been parallelized using the atom decomposition method. Equilibrium molecular dynamics method with Green-Kubo correlations is used to calculate the thermal conductivity of nanofluid. Unlike in previous studies, all interactions liquid molecule-liquid molecule, liquid molecule-solid molecule and solid atoms-solid atoms have been considered. Motion of atoms in silica nanoparticle and water molecule in the simulation domain was studied. Based on the results obtained, following conclusions may be made:

- Maxwell model and Hamilton-Crosser model under-predict the effective thermal conductivity of nanofluids. The reason that these models fail for nanofluids is that it does not take the dynamics of the nanoparticles into account.
- The results show that the density of water near the interface increases with time. This implies the generation of a double diffuse layer or the so-called hydration layer at the solid-liquid interface.
- The effective thermal conductivity of various nanofluids for our simulation shows around 25% enhancement than that of pure liquid. The enhancement compares well with previous studies.
- Lattice vibration of atoms in silica molecules is observed. Lattice vibration of atoms increases with temperature.

- It is shown that the lattice vibrations of silica nanoparticle and interfacial interaction between the nanoparticle and the liquid play important role in improving the heat transfer of the suspension.

## CHAPTER 7: FUTURE WORK

There are many other parameters which can affect the performance of nanofluids. It is important to understand the nanofluid behavior completely prior to their application in the industry. To better understand the heat transfer characteristics of nanofluids, more work should be done to understand the chemical interactions between the liquid molecules, and atoms on the surface of nanoparticles. The nanoparticles manufactured by various methods are not spherical in shape, so the effect of nanoparticle shape on heat transfer should be studied. Since these nanofluids would be used in channel flows, the near wall effect on the thermal conductivity of nanofluid should also be studied to better design the future heat transfer devices.

In the discussion of thermal transport characteristics of particle or fiber nanofluids, it is important to discuss the concept of *interfacial thermal resistance* also called *Kapitza resistance*. When heat is transferred from one phase to another, an interfacial thermal resistance can arise. Current understanding of the thermal resistance of solid-liquid interface is primarily based on the acoustic mismatch model (AMM) in which transmission and reflection of classical heat waves at the interface is considered. Since speed of sound is different in solid and liquid medium an analogy is made for the heat wave and the difference in speed at the interface causes an obstacle at the interface. The Kapitza resistance for a solid-liquid interface depends on the contact angle of the liquid or the wettability of the liquid. Barrat and Chiaruttini [2003] used EMD and NEMD and to study the interfacial resistance and the effect of wetting properties of liquid. Their results showed that the interfacial resistance is higher for a non-wetting liquid compared to a wetting



liquid. The interfacial resistance between the liquid and solid at the interface and its effect on overall heat transfer of nanofluid will be studied.

## LIST OF REFERENCES

- Ahuja A.S., J. Appl. Phys. 46(8), 855 (1975)
- Alder B. J. and Wainwright T. E., J. Chem. Phys. 31 (2), 459 (1959)
- Allen M.P., [www.fz-juelich.de/nic-series/volume23/allen.pdf](http://www.fz-juelich.de/nic-series/volume23/allen.pdf), (2004)
- Allen M.P. and Tildesley D.J., Computer Simulation of Liquids, Oxford, Oxford Science Publications (1987)
- Barrat J. and Chiaruttini F., Mol. Phys. 101(11), 1605 (2003)
- Berber S., Kwon Y. K. and Tomanek D., Phys. Rev. Lett. 84(20), 4613 (2000)
- Berendsen H.J.C., Grigera J.R. and Straatsma T.P., J. Phy. Chem. 91, 6269 (1987)
- Berendsen H.J.C., Postma J.P.M, van Gunsteren W.F., and Hermans J., Intermolecular Forces, Pullman B., Ed., Reidel, Dordrecht, p331, (1981)
- Bertolini D. and Tani A., Phys. Rev. E. 56, 4135 (1997)
- Bhattacharya P., Saha S.K., Yadav A., Phelan P.E. and Prasher R.S., J. Appl. Phys. 95, 6492 (2004).
- Brown D., Clarke J.H.R., Okuda M., and Yamazaki T., Comp. Phys. Comm. 74, 67 (1993)
- Brown D., Clarke J.H.R., Okuda M., and Yamazaki T., J. Chem. Phys. 100, 6011 (1994)
- Choi S.U.S., Development and Applications of Non-Newtonian Flows, ASME, FED-Vol. 231/MD-Vol. 66, 99-103 (1995)
- Choi S.U.S., Zhang Z.G., Yu W., Lockwood F.E., and Grulke E.A., Appl. Phys. Lett. 79(14), 2252 (2001).
- Clarke J.H.R., Smith W., and Woodcock L. V., J. Chem. Phys. 84, 2290 (1984).
- Das S.K., Putra N., Thiesen P., and Roetzel W., J. Heat Transfer 125, 567 (2003).

Demontis P., Spann S. and Suffritti G.B., J. Chem. Phys. 114, 7980 (2001)

Eastman J.A., Choi S.U.S., Li S., Soyez G., Thompson L.J., and Di Melfi R.J., Mater. Sci. Forum 312-314, 629 (1999)

Eastman J.A., Choi S.U.S., Li S., Yu W., and Thompson L.J., Appl. Phys. Lett. 78, 718 (2001)

Eastman J.A., Philpot S.R., Choi S.U.S. and Keblinski P, Annu. Rev. Mater. Res. 34, 219 (2004)

Ercolessi F., <http://www.sissa.it/furio/> (1997)

Evjen H.M., Phys. Rev. 39, 675 (1932)

Florain M., J. Chem. Phys. 106, 6082 (1997)

Gupta A., Wu X. and Kumar R., International Conference on Nanochannels, Microchannels and Minichannels, Limerick, Ireland, June 2006 (2006)

Haile J. M., Molecular Dynamics Simulation, New York, John Wiley & Sons (1997).

Hamilton R.L. and Crosser O.K., I&EC Fundamentals 1(3), 187 (1962).

Hockney R.W. and Eastwood J.W., Computer Simulations using Particles, Adam Hilger, Bristol (1988)

Jang S.P. and Choi S.U.S., Appl. Phys. Lett. 84, 4316 (2004).

Jorgensen W.L., J. Am. Chem. Soc. 103, 335 (1981)

Jorgensen W.L., J. Chem. Phys. 77, 4156 (1982)

Kalia R.K., de Leeuw S., Nakano A., and Vashishta P., Comp. Phys. Comm. 74, 316 (1993)

Kapitza P.L., J. Phys. USSR 4:181, Zh. Eksp. Teor. Fiz. 11, 1 (1941)

Keblinski P., Eggebrecht J., Wolf D., and Phillpot S.R J. Chem. Phys. 113, 282 (2000)

Keblinski P., Philpot S.R., Choi S.U.S. and Eastman J.A., Int. J. Heat & Mass Transfer 45, 855 (2002)

Kim P., Shi L., Majumdar A. and McEuen P.L., Phys. Rev. Lett. 87, 215502 (2001)

Kimura T. and Maruyama S., *Microscale Thermo. Engg.* 6(1), 3 (2002)

Knuth D., *The art of computer programming*, Addison-Wesley, Reading MA, 2nd edition, (1973)

Kohen D., Tully J. C., and Stillinger F.H., *Surf. Sci.* 397, 225 (1998)

Kramer G.J., Farragher N.P., van Beest B.W.H. and van Santen R.A., *Phys. Rev. B.* 43(6), 5068 (1991)

Kubo R., *J. Phys. Soc. of Japan*, 12(6), 570 (1957)

Lee S., Choi S.U.S, Li S. and Eastman J.A, *Trans. ASME J. Heat Transfer* 121, 280, (1999)

Lennard-Jones J.E., *Proceedings of the Royal Society (London)* 106A, 441 (1924)

Liu K.V., Choi S.U.S. and Kasza K.E., *Argonne National Laboratory Report*, ANL-88-15, (1988)

Masuda H. et al, *Netsu Bussei (Japan)* 4, 227 (1993)

Maxwell J.C., *A treatise on electricity and magnetism*, Iled, Vol. 1, Clarendon press, Oxford, U.K., 435, (1881)

McGaughey A.J.H. and Kaviany M., *Int. J. Heat and Mass Transfer* 47, 1799 (2004)

Milanova D, Wu X. and Kumar R., *2006 NSTI Nanotechnology Conference and Trade Show - Nanotech 2006*, Boston, MA, May 7-11, 2006, (2006)

Milanova D. and Kumar R., *Appl. Phys. Lett.* 87, 233107 (2005)

Milanova D., Kumar R., Kuchibhatla S. and Seal S., *Intl. Conf. on Nanochannels, Microchannels and Minichannels, ICNMM2006*, Limerick, Ireland, June 19-21, (2006)

Patel H.E., Das S.K., Sundarajan T., Nair A.S., George B. and Pradeep T., *Appl. Phys. Lett.* 83 (14), 2931 (2003)

Philippe J. and Rémi J., *Phys. Rev. B* 59, 13707 (1999)

Plimpton S., *J. Comp. Phys.* 117, 1 (1995)

Pollack G.L., Rev. Modern Phys. 41(1), 48, (1969)

Rahman A., Phys, Rev. Lett. 136, A405, (1964)

Rapaport D. C., The Art of Molecular Dynamics Simulation – 2nd ed., Cambridge, UK,  
Cambridge University Press (2004)

Sachdeva P., Wu X. and Kumar R., International Congress of Nanotechnology, San Francisco,  
USA, Sept. 2005 (2005)

Sato H., Iwama Y., Kawakilka S., Satio M., Morikami K., Yao T. and Tsutsumi S., IEEE 0-  
8186-2775-1/92 (1992)

Siegel, R.W., Annu. Rev. Mat. Sci. 21,559 (1991)

Smith G.D., <http://www.mse.utah.edu/~gdsmith/tutorials/tutorial1.ppt> (1999)

Stillinger F.H. and Rahman A., J. Chem. Phys. 60, 1545 (1974)

Stillinger F.H. and Weber T. A., Phys. Rev. B 31, 5262 (1985)

Swartz E.T. and Pohl R.O., Rev. Modern Phys. 61(3), 605 (1989)

The  $\alpha$  (low) quartz structure, <http://cst-www.nrl.navy.mil/lattice/struk/sio2a.html>

van Beest B.W.H., Kramer G.J., and van Santen R.A. Phys. Rev. Lett. 64(16), 1955 (1990)

Vassallo P., Kumar R., and D'Amico S.W., Int. J. Heat Mass Transfer 47, 407 (2004)

Verlet L., Phys. Rev. Lett. 159, 98 (1967)

Verlet L., Phys. Rev. 165(201), 214 (1968)

Vladimir V.M., J. Phys. Condens. Matter 11, 1261 (1999)

Wang X., Xu X.F., and Choi S.U.S., J. Thermophys. and Heat Transfer 13(4), 474 (1999)

Wolf D., Phys. Rev. Lett 68, 3315 (1992)

Wolf D., Keblinski P., Phillpot S.R., and Eggebrecht J., J. Chem. Phys 110, 8254 (1999).

- Woodcock L.V., *Advances in Molten Salt Chemistry*, edited by J. Braunstein, G. Mamantov, and G. P. Smith (Plenum, New York), 3, 1 (1975)
- Wu X. and Kumar R., 3rd Intl. Conf. on Microchannels and Minichannels, ICMM2005, Toronto, Canada, June 13-15, (2005)
- Wu X. and Kumar R., Keynote Lecture and Invited Paper, Proc. Nanomaterials: Synthesis, Characterization and Application, Calcutta, India, 182, Nov. 2004 (2004)
- Wu X., Sachdeva P. and Kumar R., *Appl. Phys. Lett.* (submitted) (2006)
- Xie H., Lee H., Youn W., and Choi M., *J. Appl. Phys.* 94(8), 4967 (2003)
- Xuan Y. and Li Q., *Int. J. Heat Fluid Flow* 21, 158 (2000)
- Xue L., Keblinski P., Philpot S.R., Choi S.U.S. and Eastman J.A., *J. Chem. Phys.* 118(1), 337 (2003)
- Xue L., Keblinski P., Philpot S.R., Choi S.U.S. and Eastman J.A., *J. Heat Mass Tr.* 47, 4277 (2004)
- Young H.L., Biswas R., Soukoulis C.M., Wang C.Z., Chan C.T., and Ho K.M., *Phys. Rev. B* 43, 6573 (1991)
- Yu C. J., Richter A.G., Datta A., Durbin M.K. and Dutta P., *Phys. B* 283,27 (2000)
- Yu W. and Choi S.U.S., *J. Nanoparticle Res.* 5, 167 (2003)